sustainability

MDPI

Article

A Comprehensive Assessment of $PM_{2.5}$ and PM_{10} Pollution in Cusco, Peru: Spatiotemporal Analysis and Development of the First Predictive Model (2017–2020)

Julio Warthon, Ariatna Zamalloa *, Amanda Olarte, Bruce Warthon, Ivan Miranda, Miluska M. Zamalloa-Puma, Venancia Ccollatupa, Julia Ormachea, Yanett Quispe, Victor Jalixto, Doris Cruz, Roxana Salcedo, Julieta Valencia, Mirian Mio-Diaz, Ruben Ingles, Greg Warthon, Roberto Tello, Edwin Uscca, Washington Candia, Raul Chura, Jesus Rubio and Modesta Alvarez

Centro de Investigación de Energía y Atmósfera, Universidad Nacional de San Antonio Abad del Cusco, Cusco 08003, Peru; julio.warthon@unsaac.edu.pe (J.W.); amanda.olarte@unsaac.edu.pe (A.O.); 160531@unsaac.edu.pe (B.W.); 150353@unsaac.edu.pe (I.M.); miluska.zamalloa@unsaac.edu.pe (M.M.Z.-P.); venancia.ccollatupa@unsaac.edu.pe (V.C.); julia.ormachea@unsaac.edu.pe (J.O.); yanett.quispe@unsaac.edu.pe (Y.Q.); victor.jalixto@unsaac.edu.pe (V.J.); 234301@unsaac.edu.pe (D.C.); 224103@unsaac.edu.pe (R.S.); nazaria.valencia@unsaac.edu.pe (J.V.); 144235@unsaac.edu.pe (M.M.-D.); ruben.ingles@unsaac.edu.pe (R.I.); 234530@unsaac.edu.pe (G.W.); 103669@unsaac.edu.pe (R.T.); thelosius@gmail.com (E.U.); washington.candia@unsaac.edu.pe (W.C.); pastor.chura@unsaac.edu.pe (R.C.); jesus.rubio@unsaac.edu.pe (J.R.); esther.alvarez@unsaac.edu.pe (M.A.)

* Correspondence: 182773@unsaac.edu.pe

Abstract: This study presents the first comprehensive assessment of air pollution by $PM_{2.5}$ and PM_{10} in the city of Cusco, aiming to determine atmospheric pollution levels, characterize air quality, and develop predictive models. The research, conducted during 2017–2020, systematically evaluated particulate matter (PM) contamination using a high-volume sampler (HiVol ECOTEC 3000) installed at 18 monitoring sites distributed across five urban districts. Multiple linear regression (MLR) models were developed and evaluated, incorporating meteorological, seasonal, and temporal variables under two approaches: direct linear (Model 1) and logarithmic transformation (Model 2). The model evaluation employed R^2, RMSE, MAE, MAPE, IOA, and CV statistical indicators. The results revealed concentrations significantly exceeding WHO guideline values, with $PM_{2.5}$ ranging between 41.10 ± 3.2 μg/m^3 (2020) and 82.01 ± 5.1 μg/m^3 (2018), while PM_{10} values ranged from 45.07 ± 2.8 μg/m^3 (2020) to 72.35 ± 4.3 μg/m^3 (2017). A notable reduction was observed during 2020, attributable to COVID-19 pandemic restrictions. The Air Quality Index (AQI) indicated predominantly "Unhealthy" and "Very Unhealthy" levels during 2017–2018, improving to "Unhealthy for Sensitive Groups" in 2020. MLR models achieved maximum efficiency using logarithmic transformation, obtaining $R^2 = 0.98$ ($p < 0.001$) for $PM_{2.5}$ in the 2020 rainy season and $R^2 = 0.44$ ($p < 0.001$) for PM_{10} in the 2018 annual model. These findings demonstrate the existence of nonlinear relationships between pollutants and predictor variables in Cusco's atmospheric basin.

Keywords: particulate matter; concentration; $PM_{2.5}$; PM_{10}; predictive model; linear regression; air quality index

check for updates

Academic Editor: Harvey Hou

Received: 5 December 2024
Revised: 31 December 2024
Accepted: 2 January 2025
Published: 7 January 2025

Citation: Warthon, J.; Zamalloa, A.; Olarte, A.; Warthon, B.; Miranda, I.; Zamalloa-Puma, M.M.; Ccollatupa, V.; Ormachea, J.; Quispe, Y.; Jalixto, V.; et al. A Comprehensive Assessment of $PM_{2.5}$ and PM_{10} Pollution in Cusco, Peru: Spatiotemporal Analysis and Development of the First Predictive Model (2017–2020). *Sustainability* **2025**, *17*, 394. https://doi.org/10.3390/su17020394

Copyright: © 2025 by the authors. Licensee MDPI, Basel, Switzerland. This article is an open access article distributed under the terms and conditions of the Creative Commons Attribution (CC BY) license (https://creativecommons.org/licenses/by/4.0/).

1. Introduction

Air pollution is a significant public health and environmental problem in cities where fossil fuel-based motor transport is developed due to increasing population, motorization,

and industrialization [1–11]. Chronic exposure to air pollutants, especially particulate matter, has been associated with increased morbidity and mortality from cardiovascular, cerebrovascular, respiratory diseases, and lung cancer [12–24]. In 2019, air pollution caused more than six million premature deaths globally [25,26]. In the Americas, approximately 250,000 deaths annually are attributed to urban air pollution [27].

Particulate matter (PM) is considered one of the most hazardous air pollutants for health [7,14,28–35]. The EPA defines particulate matter as a mixture of solid and liquid particles suspended in the air, varying in size, chemical composition, and origin [36]. They are classified into coarse (≤10 µm), fine (≤2.5 µm), and submicron (≤1 µm) particles. The smallest particles carry a greater risk to health due to their ability to penetrate deeply into the respiratory and circulatory systems [36–39]. Chronic exposure to PM is related to inflammation and bronchial hyperreactivity, exacerbating asthma, COPD, and other obstructive diseases [40–42]. It also induces oxidative stress, endothelial dysfunction, atherosclerosis, and coagulation disorders [14,15,43–45].

In 2021, the World Health Organization (WHO) published new Global Air Quality Guidelines, setting stricter limits for $PM_{2.5}$ and PM_{10}. The guideline level for $PM_{2.5}$ is 15 $\mu g/m^3$ as a 24 h average and 5 $\mu g/m^3$ as an annual average. For PM_{10}, it is 45 $\mu g/m^3$ for a 24 h time average and 15 $\mu g/m^3$ for an annual average [46]. These values are lower than those of 2005, which set maximum levels for $PM_{2.5}$: 25 $\mu g/m^3$ (24 h) and 10 $\mu g/m^3$ (annual), and for PM_{10}: 50 $\mu g/m^3$ (24 h) and 25 $\mu g/m^3$ (annual) [47]. The new guidelines are based on recent toxicological and epidemiological evidence [48]. On the other hand, the US EPA Air Quality Index (AQI) is a vital tool for communicating the risks of air pollution. It covers six principal pollutants, including $PM_{2.5}$ and PM_{10}, on a scale of 0 to 500, with six health categories. The AQI translates technical data into understandable information, facilitating informed decisions about exposure to polluted air [49–51].

Air pollution has become one of the most pressing challenges in developing countries, particularly in Latin America [52]. This problem affects human health, the economy, and cultural heritage, increasing medical expenses and damaging historical buildings and monuments [53]. In Peru, the lack of systematic information on the actual levels of air pollution in most cities highlights the importance of previous studies in this field [54,55]. Cusco, the historic capital of the Peruvian Andean region, was declared a World Heritage Site by UNESCO in 1983 [56,57] and is no exception to this problem. With its rich Inca and colonial history, Cusco is home to numerous monuments of global importance that are vulnerable to the effects of air pollution. Acid deposition and suspended particulate matter can accelerate the erosion and deterioration of these archaeological sites and colonial structures [58,59]. The geographic location of the city in a high-altitude valley, coupled with an unregulated vehicle fleet, domestic biomass combustion, waste burning, and other anthropogenic activities, has led to air pollutant levels exceeding established ECAs [60,61].

Air quality assessment is essential in the city of Cusco for public health and environmental reasons, and predictive tools are being developed to help mitigate its impacts. Various statistical methods have been applied in meteorological studies to predict particulate matter concentrations in recent years. Among these, the multiple linear regression method has stood out as one of the most preferred and widely used techniques for years [62–66]. Although other statistical models exist, multivariate linear regression (MLR) has proven particularly effective and reliable in recent studies [67]. An example is the study by Zhao et al. [68], who employed a multivariate linear regression (MLR) model to examine the relationship between meteorological factors and air pollutants in Beijing. Their $PM_{2.5}$ concentration prediction model demonstrated remarkable effectiveness, with coefficients of determination (R^2) of 0.766, 0.852, and 0.874 for the annual, spring, and summer time scales of 2015, respectively. These results indicate a high predictive ability of the model,

especially at the seasonal time scales. Srivastava et al. [69] conducted research incorporating machine learning techniques in New Delhi. They used meteorological parameters such as vertical wind, wind speed and direction, temperature, and relative humidity to predict the concentrations of CO, NO_2, O_3, SO_2, PM_{10}, and $PM_{2.5}$ at three strategic sites. Their study employed methods such as linear regression, stochastic gradient descent regression, multilayer perceptron, and gradient boosting regression, evaluating the performance of the models using metrics such as MSE, MAE, and R [70]. On the other hand, Ke et al. [71] developed a more comprehensive approach with an automated air quality forecasting system based on a combination of models, including MLR, MLP, RF, GBPT, and SVR. This system, designed to forecast six common pollutants daily ($PM_{2.5}$, PM_{10}, SO_2, NO_2, O_3, and CO), integrates machine learning models and an ensemble model supported by an extensive knowledge base. Using five years of data (2015–2019) from seven major cities in China, they demonstrated that their automated system can achieve efficient forecasting performance. In a different geographical context, Zateroglu [66] conducted a study in an urban area of Turkey using data collected over five years (2011–2015). His approach combined multiple linear regression with principal component analysis to analyze air pollutant concentrations and climate data. Various performance indicators such as RMSE, NMSE, CV, FB, and IOA verified the model's accuracy, revealing acceptable values and demonstrating the model's feasibility in predicting pollutant concentrations. These studies exemplify the diversity of approaches and the effectiveness of regression and machine learning models in different geographic contexts. Along these lines, choosing a multiple linear regression-based approach for our study in Cusco aligns with current trends in air quality forecasting methods [72]. For our research, the ability of this method to handle multiple predictor variables is crucial, given that the deposition, dispersion, and transport of air pollutants are strongly influenced by regional climatic conditions [73,74]. Cusco presents unique geographic and climatic characteristics that justify a specific approach to studying air pollution. Our study aims to analyze the spatiotemporal trends of $PM_{2.5}$ and PM_{10} in Cusco between 2017 and 2020 and to develop the first predictive model based on multiple linear regression for these particles in the city. This model uses meteorological variables as predictors, recognizing the importance of optimizing estimates for seasonal periods.

Despite the importance of Cusco as a cultural heritage site and a major tourist destination in Peru, with over four million visitors annually [75,76], there is a notable shortage of systematic data on air quality in the city. This lack of information, coupled with Cusco's unique characteristics as a high-altitude city and its vulnerability to deterioration due to air pollution, makes it imperative to develop studies that determine current pollution levels and predict future concentrations. Implementing a monitoring and prediction system adapted to the specific conditions of Cusco is essential to protect public health and cultural heritage. In this context, the present study aims to address these critical needs through the following objectives. The main objective of this study is to evaluate, for the first time, $PM_{2.5}$ and PM_{10} concentrations at several representative sites in the city of Cusco between 2017 and 2020. Monitoring was carried out with EPA-certified high-volume sampling equipment [61].

The specific objectives were (1) to determine the average daily concentrations of $PM_{2.5}$ and PM_{10} and their spatiotemporal variability; (2) to compare these concentrations with WHO air quality standards and calculate AQI levels according to the US-EPA; and (3) to build and identify the best model to estimate particulate matter concentration based on meteorological variables.

2. Materials and Methods

2.1. Study Area

The study area selected for this research is Cusco, the historic capital of Peru (−13.52° S, −71.98° W), recognized as a cultural heritage of humanity. Cusco receives millions of tourists annually because it houses one of the world's seven wonders, Machu Picchu. Located in the Andes Mountains, at approximately 3400 m above sea level, it has a population of more than 430,000 inhabitants [77]. The city has two well-defined types of climate: a dry season from April to October and a rainy season from November to March.

For this study, 18 representative monitoring sites were selected in Cusco, including the historic center. These sites were located mainly near avenues with high vehicular and pedestrian traffic. Figure 1 illustrates the location of these sites on a city map. The selection of monitoring sites was based on criteria established in the EPA protocols for monitoring particulate matter air pollution [78,79]. These criteria included the representativeness of vehicle emission sources, the proximity to populations potentially exposed to air pollutants, the safety and accessibility of equipment, and the availability of electrical supply. On the National University of San Antonio Abad del Cusco (UNSAAC) campus, site S1 at the Faculty of Education represents a quiet environment. In contrast, sites S3 (Gate 5), S15 (Gate 3), S16 (Faculty of Economics), S17 (Faculty of Tourism), and S18 (Tricentenario Square) reflect the interaction between university life and the surrounding urban dynamism. Residential areas such as site S2 (APV Paraiso de Fátima) in San Sebastian offer a perspective of an area influenced by its proximity to the brick industry. S4 (Clorinda Matto de Turner School) and S14 (San Jeronimo Health Center) combine their locations, facing high vehicular traffic and brick factories, respectively. In the Wanchaq district, S5 (Municipality) and S6 (Wanchaq Health Center) represent municipal activity and medical assistance nodes developed near high vehicular traffic. In the historical center, the emblematic squares and streets S7 and S8 (San Francisco Square), S9 (San Blas Square), S10 (Limacpampa Square), S11 (Pumacchupan Square), and S12 (Matara Street) show the interaction between cultural heritage, tourism, and high vehicular traffic. Site S13 (Belen Pampa Health Center) in Santiago stands out for its location near streets with low pedestrian and regular vehicular traffic. This diversity of measurement sites provides a comprehensive understanding of Cusco's complex interactions between built environments, human activities, and vehicular traffic, allowing for detailed air quality analyses in different urban contexts.

2.2. Overview Study

$PM_{2.5}$ and PM_{10} measurements were carried out over three years (2017, 2018, and 2020), following a rigorous methodological protocol. This process included collecting, preprocessing, and selecting particle data and meteorological variables. The particle concentrations obtained by year and monitoring site were subsequently compared with WHO guidelines [46,47]. The Air Quality Index was also calculated by monitoring sites and districts. Finally, a model was built, and its performance was evaluated. This study includes a multiple linear regression (MLR) model, which is subdivided into two models: (Model I) without any transformation and (Model II) with the variable to be predicted transformed by logarithm. The performance of each model was evaluated throughout each year, and during the entire study period for each season. The best model was selected based on various evaluation metrics to estimate $PM_{2.5}$ and PM_{10} concentrations in Cusco. In addition, the virtues and limitations of the models are disclosed. Figure 2 schematically illustrates the methodology used in this research. In this research, the Python programming language and its respective libraries were used to analyze and statistically evaluate the data, as well as for all preprocessing and model development.

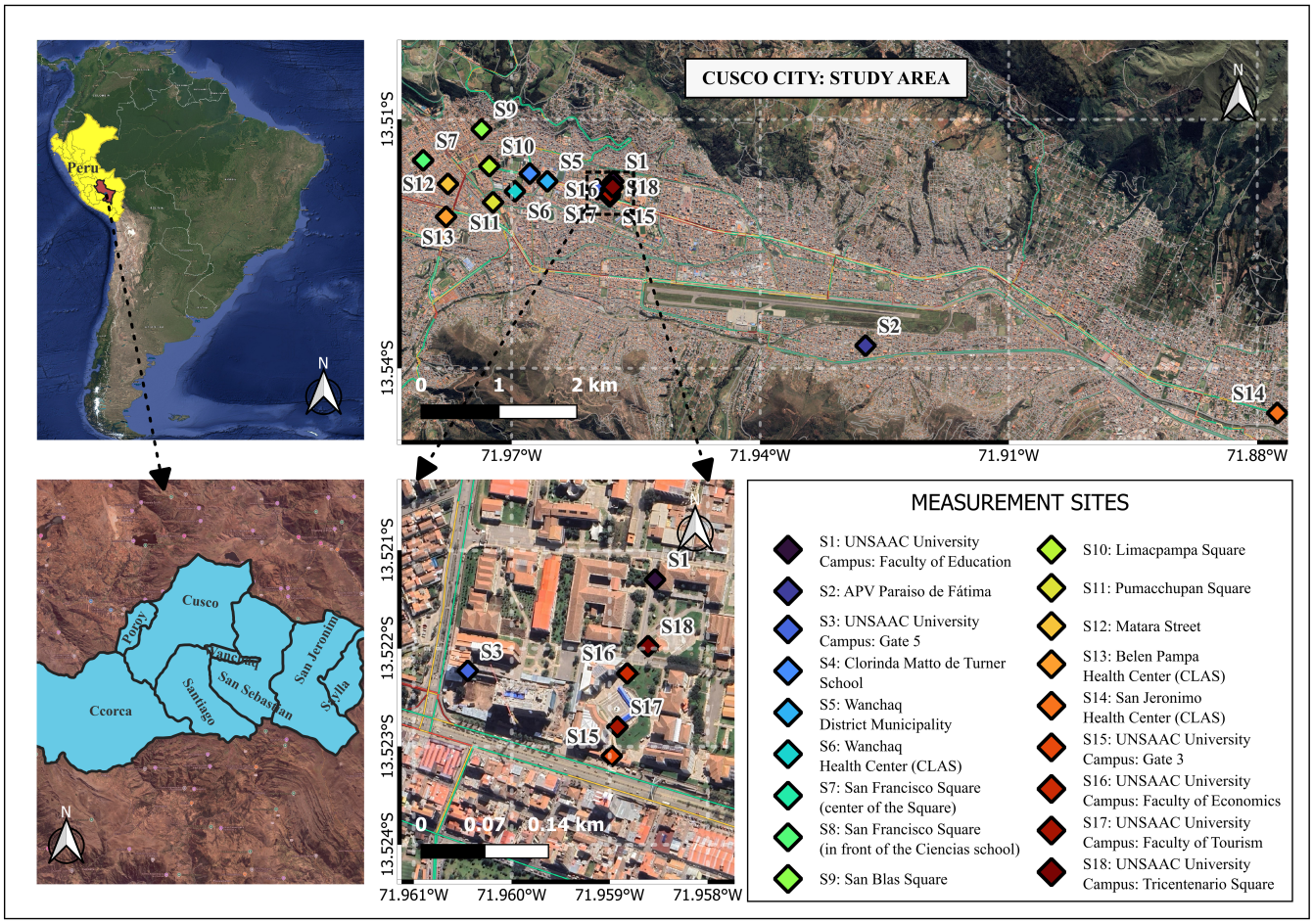


Figure 1. The distribution map of monitoring sites in the Cusco study area.

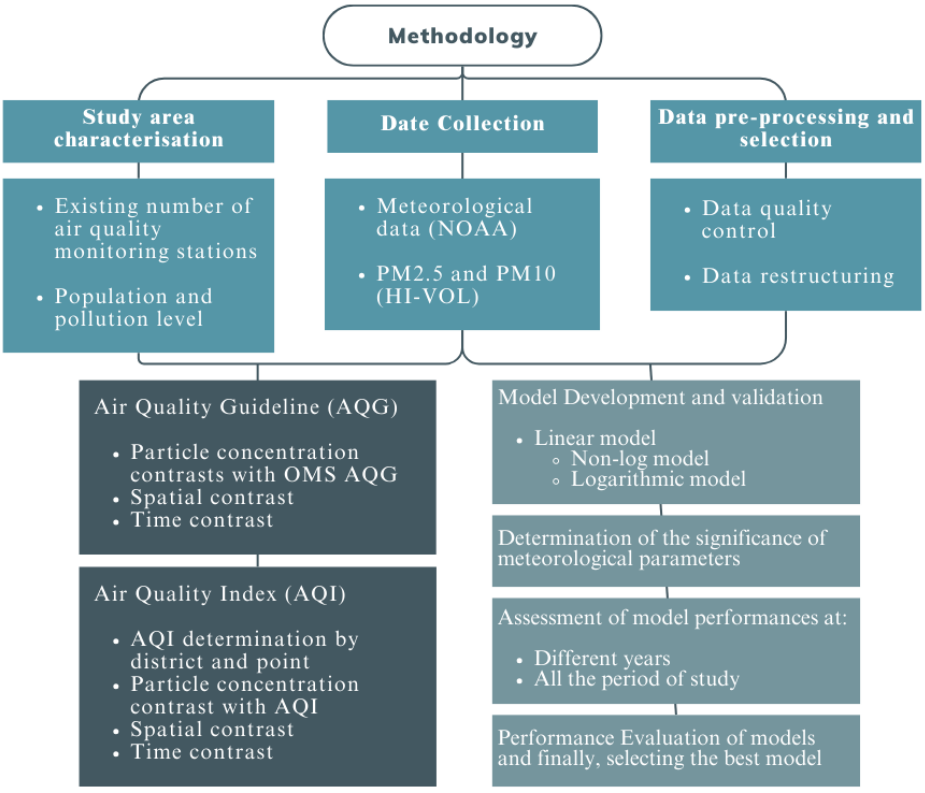


Figure 2. A schematic representation of the methodology.

2.3. PM and Meteorological Data

This study used two datasets: (I) $PM_{2.5}$ and PM_{10} concentration data and (II) NOAA meteorological data. $PM_{2.5}$ and PM_{10} concentrations were measured at the previously indicated sites using a HiVol Ecotech 3000 high-volume monitor. Measurements were made over three study years (2017, 2018, and 2020), recording the assessment date (DATE) and the daily particle concentration expressed in $\mu g/m^3$ (see Supplementary Materials). Daily meteorological data were obtained from the NOAA satellite for the same period, covering the following parameters: mean temperature, T (°C); maximum temperature, MAXT (°C); minimum temperature, MINT (°C); relative humidity, RH (%); precipitation, PREC (mm); wind speed, WS (m/s); wind direction, WD (°), and atmospheric pressure, PRES (hPa).

Collection and Quantification of Particulate Matter

Measurements were taken at each site over different periods in 2017, 2018, and 2020. A high-volume sampler (HiVol-3000, Ecotech, Australia) with $PM_{2.5}$ and PM_{10} headers collected 24-h daily samples on 8 × 10-inch Whatman-UK quartz filters [61,80]. The operating flow was 67 m^3/h, allowing for daily volumes of approximately 1600 m^3 to be obtained. Quartz filters were conditioned for 24 h before and after sampling at a controlled temperature and humidity in a desiccator containing silica gel desiccant, which was replaced at each monitoring campaign [81,82]. Gravimetric analysis was performed using an Ohaus analytical balance with a sensitivity of 0.0001 g, applying US-EPA Compendium Method IO-3.1 [83–85]. PM concentrations ($\mu g/m^3$) were calculated using the following equation:

$$C = \frac{m}{V_{std}} \quad (1)$$

where (m) is the mass ratio of the pollutant obtained from the gravimetric methodology $(m_f - m_i)$ and (V_{std}) is the standardized volume of filtered air. The standard volume has, by definition, the following equation:

$$V_{std} = V_s \frac{P_{atm}}{P_{std}} \frac{T_{std}}{T_{atm}} \quad (2)$$

T_{atm} is the atmospheric temperature measured with mercury thermometers (Hg), and p_{atm} is the atmospheric pressure measured with a Mesa Labs brand flowmeter, model FlexCal; both variables were recorded in Cusco. The standard variables, obtained from the protocol established by the EPA [86,87], are the standard temperature (T_{std}), with a value of 298 K, and the standard pressure (p_{std}), with a value of 760 mmHg. The accumulated uncorrected sample volume of air (V_s) in the city of Cusco, at an altitude of 3347 masl, was obtained using the following equation:

$$V_s = Q \cdot t \quad (3)$$

The high-volume sampler measures the flow rate (Q) in real-time. The atmospheric airflow through the sampling equipment was 67 m^3/h, which remained approximately constant for 24 h.

2.4. Data Preprocessing

Data quality control is essential to ensure the reliability of the results and prevent overfitting or underfitting problems [88]. This study applied a preprocessing process to all collected data on particulate matter and meteorological parameters, which were subsequently used to assess $PM_{2.5}$ and PM_{10} concentrations, calculate AQI, and construct predictive models. Preprocessing included removing duplicate data from the same day, followed by median imputation of outlier data for each variable [89]. The aim was to

maintain the available data, since there is a limited number of data for model construction [90,91]. After applying these filters, 128 valid records for $PM_{2.5}$ and 103 for PM_{10} were obtained. These cleaned datasets were used uniformly in all phases of the study, ensuring the consistency of the analysis.

2.5. Air Quality Standard (AQG) and Air Quality Index (AQI)

The particulate matter assessment results were compared with the World Health Organization (WHO) Air Quality Standard (AQG) for each year, district, and monitoring site. Likewise, the Air Quality Indices (AQIs) were calculated from these assessments, following the indications stipulated in the EPA documentation [92]. In this study, AQIs were determined (I) by monitoring site and (II) by district for both cases throughout the study period. See Figures 8 and 9. The 2005 WHO AQG sets limits of 25 $\mu g/m^3$ for $PM_{2.5}$ and 50 $\mu g/m^3$ for PM_{10} over a 24 h period. As of 2021, the WHO AQG has been reduced to 15 $\mu g/m^3$ for $PM_{2.5}$ and 45 $\mu g/m^3$ for PM_{10}. The EPA AQI is classified into five levels according to the degree of harm to human health: Good (0–50), Moderate (51–100), Unhealthy for Sensitive Groups (101–150), Unhealthy (151–200), Very Unhealthy (201–300), and Hazardous ($\geq$301) [93].

A Python script was developed to calculate the quality indices. This script takes the maximum values of each monitoring site, as recommended by the EPA [93], and uses the following equation:

$$I_p = \frac{I_{Hi} - I_{Lo}}{BP_{Hi} - BP_{Lo}}(C_p - BP_{Lo}) + I_{Lo} \quad (4)$$

where:

- C_p is the truncated concentration of contaminant p;
- BP_{Hi} is the cut-off site of the concentration that is greater than or equal to C_p;
- BP_{Lo} is the cut-off site of the concentration that is less than or equal to C_p;
- I_{Hi} is the AQI value corresponding to BP_{Hi};
- I_{Lo} is the AQI value corresponding to BP_{Lo}.

Truncation values for each particle concentration level are referenced in the guidance established by the EPA [94].

2.6. Selection of Significant Variables

Three new variables were created from the evaluation date of the concentration of particulate matter: (I) the day of the week (DS), which runs from Monday to Sunday, coded from 1 to 7 according to the corresponding day; (II) work or non-work day (DL), where work is 1, and non-work is 2; and (III) season (Season), dry (1) and rainy (2). The study period divided each year into two seasons: dry (April to October) and rainy (November to March), both for $PM_{2.5}$ and PM_{10} and for meteorological parameters. In addition, the assumptions required by the multiple linear regression (MLR) model were verified. A correlation matrix was created to observe the multicollinearity between the predictors and the linear relationship between each predictor and the variable to be predicted. Likewise, Shapiro–Wilk tests were carried out, and QQ-Plot graphs were used to verify the normality of the data.

2.7. Multiple Linear Regression Model Development

The $PM_{2.5}$ and PM_{10} datasets, once the above assumptions were verified, were divided into two parts: 80% of the data was used to train the model, and the remaining 20% was used to test its performance [95,96]. A multiple linear regression (MLR) model was used, divided into two versions: (I) without transformation (model 1) and (II) with the variable to

be predicted transformed (model 2). The MLR model assumes a linear relationship between the variable to be predicted and the predictors. The equations of the models are as follows:

Model 1:

$$PM_{2.5} = \beta_0 + \beta_1 * x_{i1} + \beta_2 * x_{i2} + \ldots + \beta_p * x_{ip} + \epsilon \quad (5)$$

$$PM_{10} = \beta_0 + \beta_1 * x_{i1} + \beta_2 * x_{i2} + \ldots + \beta_p * x_{ip} + \epsilon \quad (6)$$

Model 2:

$$\log(PM_{2.5}) = \beta_0 + \beta_1 * x_{i1} + \beta_2 * x_{i2} + \ldots + \beta_p * x_{ip} + \epsilon \quad (7)$$

$$\log(PM_{10}) = \beta_0 + \beta_1 * x_{i1} + \beta_2 * x_{i2} + \ldots + \beta_p * x_{ip} + \epsilon \quad (8)$$

where:

- β_0 is a constant value corresponding to the interaction;
- $\beta_1, \beta_2, \ldots, \beta_p$ are partial regression coefficients;
- x_{i1} to x_{ip} are the predictor variables;
- ϵ is the residual or error, the difference between the observed value and the one estimated by the model;
- $\log(PM_{2.5})$ and $\log(PM_{10})$ are the logarithmic transformations of the variables to be predicted.

For RLM models to be valid and perform well, they must meet the following conditions:

- There is no collinearity or multicollinearity between predictors.
- A linear relationship between the predictors and the variable to be predicted.
- A normal distribution of residuals.
- Homoscedasticity of the residuals means that the variance of the variable to be predicted must be constant throughout the range of predictors.

A heatmap was made with the Pearson correlation coefficient to verify these conditions and observe multicollinearity and linear relationships between variables. A residual diagnosis was performed to verify normal distribution and homoscedasticity, including a normal Q-Q plot and a residual plot. The Q-Q plot compares theoretical data from a normal distribution to actual data, and for the residuals to be normally distributed, they must match the 45° slope. The homoscedasticity plot shows the residuals on the Y-axis and the predicted values on the X-axis. Although these theoretical assumptions must be met, real-world data do not always fully satisfy them. In [97], it is mentioned that slight variations in these assumptions can be accepted. To validate the normality of the data, the Shapiro–Wilk test was also performed, which indicates that a p-value less than 0.05 suggests that normality is met; otherwise, it is rejected. In this study, numerical variables and categorical variables transformed into numerical data were used, such as day of the week (DS), working or non-working day (DL), and dry or rainy season (Season).

2.8. Model Evaluation Metrics

In this study, six metrics were used to evaluate the constructed models: Root Mean Square Error (RMSE), Normalized Mean Square Error (NMSE), Mean Absolute Error (MAE), Mean Absolute Percentage Error (MAPE), Index of Agreement (IOA) and Coefficient of Variation (CV). Table 1 shows the mentioned metrics.

The selection of models was based on the results obtained from the different evaluation metrics of each model.

Table 1. Statistical Indicators for Model Performance Evaluation.

Statistical Indicator	Formula	Ideal Value
Root Mean Square Error	$RMSE = \sqrt{\frac{\sum(PM_E - PM_O)^2}{n}}$	0
Normalized Mean Square Error	$NMSE = \frac{\sum(PM_O - PM_E)^2}{\overline{PM_O} \cdot \overline{PM_E}}$	0
Mean Absolute Error	$MAE = \frac{\sum(PM_E - PM_O)^2}{n}$	0
Mean Absolute Percentage Error	$MAPE = \frac{\sum \lvert \frac{PM_E - PM_O}{PM_O} \rvert}{n} \times 100\%$	0
Index Of Agreement	$IOA = 1 - \frac{\sum(PM_E - PM_O)^2}{\sum[\lvert PM_E - \overline{PM_O} \rvert + \lvert PM_O - \overline{PM_O} \rvert]^2}$	1
Coefficient of Variation	$CV = \frac{\sqrt{\frac{\sum(PM_E - PM_O)^2}{n}}}{\overline{PM_O}}$	0

Where PM_E is estimated particulate matter and PM_O is observed particulate matter.

3. Results and Discussion

3.1. Evaluation of Particulate Matter and Meteorological Data

In Figure 3, the distribution of the $PM_{2.5}$ concentration measured during the different years of study is observed. It can be seen that the concentration averages are similar between the years 2017 and 2018. However, in 2020, a considerable reduction was recorded. In 2018, with 49 samples, an average of 82.01 $\mu g/m^3$ was obtained, representing an increase of 5.91% compared to 2017, with 29 samples with an average of 77.46 $\mu g/m^3$. On the other hand, in 2020, with 50 samples, an average of 41.10 $\mu g/m^3$ was recorded, indicating a reduction of 46.94% and 49.88% compared to the years 2017 and 2018, respectively. This significant decrease in $PM_{2.5}$ concentration is attributed to the confinement period due to the COVID-19 pandemic, which resulted in lower emissions of air pollutants [61,98]. In Figure 3b, similar behavior is shown for PM_{10} in the three years of study. In 2017, with 31 samples, an average of 72.35 $\mu g/m^3$ was recorded, representing 8.87% higher than the average for 2018, with 42 samples having an average of 65.93 $\mu g/m^3$. In 2020, with 30 samples, 37.72% and 31.65% were reduced compared to 2017 and 2018. These findings align with a global trend observed in numerous international studies investigating the impact of lockdown measures on urban air quality. For example, Kumar et al. [99] reported reductions in $PM_{2.5}$ concentrations ranging from 19% to 54% in five major cities in India. Cities with higher traffic volumes were found to show more significant reductions. Similarly, Sharma et al. [100] observed reductions of 43% and 31% in $PM_{2.5}$ and PM_{10}, respectively, in a study covering 22 cities in different regions of India. These percentages are remarkably close to those observed in Cusco, indicating that the impact of the lockdown in our city was comparable to that experienced in India. It is interesting to note that the study by Wang P. et al. [101] in Chinese cities showed absolute reductions in $PM_{2.5}$ concentrations ranging from 5.35 to 30.79 $\mu g/m^3$. The magnitude of the change observed in Cusco, a reduction of approximately 40 $\mu g/m^3$ for $PM_{2.5}$, suggests an even more significant impact than that observed in some of the larger Chinese metropolises. The global study by Benchrif et al. [102] covered 21 cities worldwide. In contrast to our results, the reduction observed in Cusco (approximately 47–50% for $PM_{2.5}$) stands out significantly, ranking among the most pronounced worldwide. Our findings are comparable to those recorded in cities that experienced the most significant improvements in air quality, such as Islamabad (−60%), Abu-Dhabi (−52%), and Lima (−46%), the latter particularly relevant as it is also a

Peruvian city. It is notable that the decrease in Cusco far exceeds the minimal reductions observed in other cities such as Dhaka (−7%), Manama and Kampala (−9%), Bogotá (−10%) and Algiers (−11%).

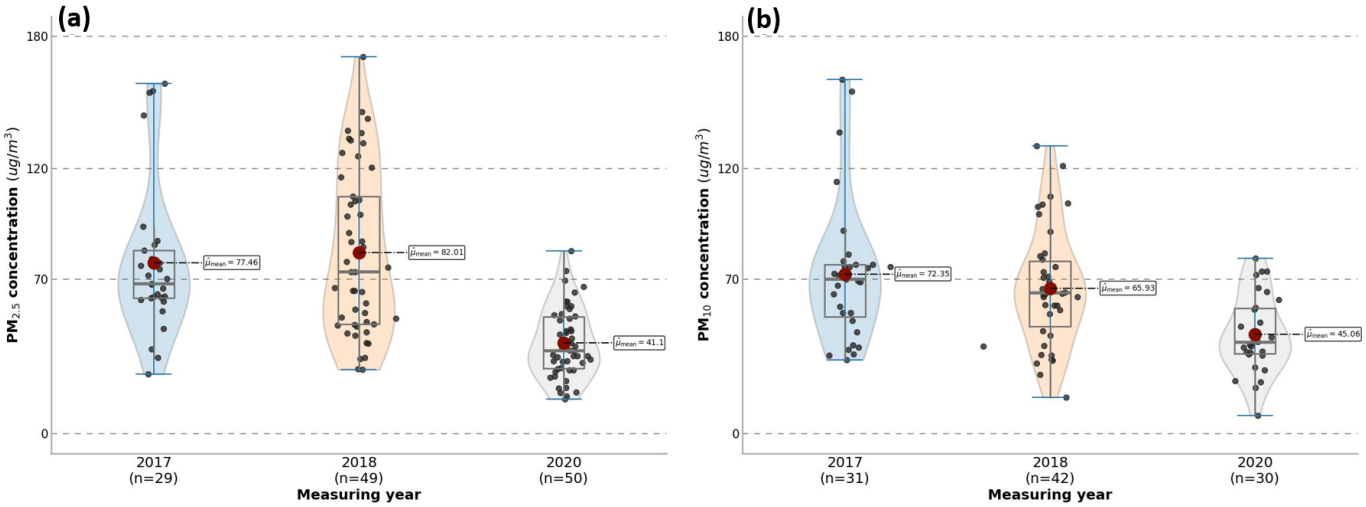


Figure 3. The Violin–Plox concentration of particulate matter during the study years 2017, 2018, and 2020. (**a**) $PM_{2.5}$; (**b**) PM_{10}.

Figure 4 shows the relationship between the target air pollutant and each meteorological variable. In 2017 (a), there were four significant variables, all negatively associated with the target pollutant: mean temperature (T °C) with a Pearson coefficient of −0.45, minimum temperature (MINT °C) with a Pearson coefficient of −0.69, relative humidity (RH%) with a Pearson coefficient of −0.63, and wind speed (WS m/s) with a Pearson coefficient of −0.39. However, in 2018 (b), there were only three significant variables, two positively associated and one negatively related with the target pollutant: maximum temperature (MAXT °C) with a Pearson coefficient of 0.31, relative humidity (RH%) with a Pearson coefficient of −0.43, and atmospheric pressure (PRES hPa) with a Pearson coefficient of 0.31. Finally, in 2020 (c), there were two significant variables, both negatively associated with the target variable: relative humidity (RH%) with a Pearson coefficient of −0.31, and atmospheric pressure (PRES hPa) with a Pearson coefficient of −0.54. The association between PM_{10} and $PM_{2.5}$ with meteorological parameters is similar.

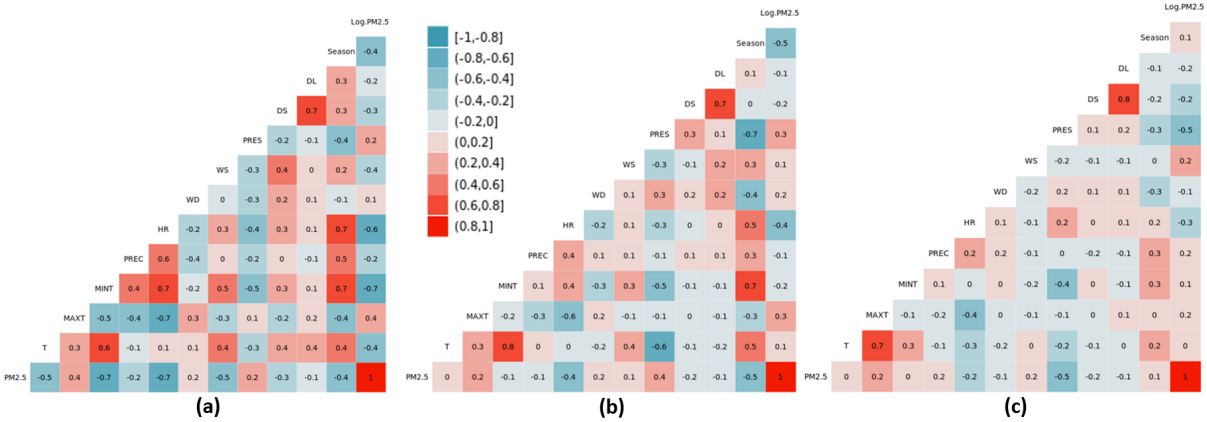


Figure 4. Heatmap of correlation for each year of study between $PM_{2.5}$ and meteorological parameters. (**a**) Heatmap for 2017; (**b**) Heatmap for 2018; (**c**) Heatmap for 2020.

The variation in $PM_{2.5}$ and PM_{10} concentrations over 2017, 2018, and 2020 reveals interesting patterns that correlate with changes in meteorological variables and significant

external events. Similar levels of $PM_{2.5}$ were observed in 2017 and 2018, with a slight increase of 5.91% in 2018 compared to 2017. Changes in the associations between the pollutant and meteorological variables could explain this moderate increase. In 2017, four meteorological variables showed significant negative associations with $PM_{2.5}$: mean temperature, minimum temperature, relative humidity, and wind speed. These relationships suggest that warmer, more humid, and windy conditions tend to reduce $PM_{2.5}$ concentrations. In 2018, the pattern changed markedly. Atmospheric pressure showed a positive association with $PM_{2.5}$, while relative humidity maintained a negative association, albeit weaker than in 2017. This change could explain the slight increase in $PM_{2.5}$ concentrations, as higher atmospheric pressure conditions appear to favor particle accumulation. For PM_{10}, the trend was opposite between 2017 and 2018, with a decrease of 8.87% in concentrations. This difference suggests that meteorological factors may affect particles of different sizes differently due to differences in the formation, dispersion, and deposition processes. In 2020, a drastic decrease in $PM_{2.5}$ and PM_{10} concentrations was observed compared to 2017 and 2018, mainly attributed to the lockdown due to the COVID-19 pandemic. However, the relationships with meteorological variables also changed significantly. In 2020, only relative humidity and atmospheric pressure showed significant associations with $PM_{2.5}$, both negative. The persistence of the negative association with relative humidity over the three years suggests that this factor plays a consistent role in reducing $PM_{2.5}$ concentrations, possibly through wet deposition. This indicates that mitigation strategies could be essential during dry seasons.

Figure 5 shows a complex interaction between meteorological parameters and $PM_{2.5}$ concentration. In Figure 5a, the average temperature tends to be negatively associated with $PM_{2.5}$ pollution, with low values recorded between January and August, while between September and November, with higher temperatures, concentrations decrease. This pattern is similar for both maximum and minimum temperatures. Relative humidity and precipitation also negatively affect $PM_{2.5}$ concentration. Humidity decreases from April to November, while during the increase between December and March, a decrease in particulate matter is observed. Precipitation negatively correlates with $PM_{2.5}$ concentration, with high values between December and March and low values between April and October. Atmospheric pressure shows a positive trend with $PM_{2.5}$ concentration, with higher values between April and September and lower values between October and March. This relationship could be linked to high- and low-pressure systems that affect atmospheric stability and, therefore, the dispersion of pollutants [103]. Wind speed is an essential factor in the dispersion of particulate pollution. It is negatively associated with $PM_{2.5}$ concentration, with high values from July to December and low values from January to June. Both wind speed and direction directly influence the dispersion of $PM_{2.5}$ and PM_{10} particles. In some areas with turbulent flow, the dispersion is more significant. However, due to the city's geography, the flow follows the predominant wind direction, Southwest. On the other hand, the analysis of the wind rose shows a more significant presence of winds in the North–South and Northeast–Southwest directions. In contrast, winds are minimal between the Southeast and Northeast directions. In Figure 5b, it can be observed that the association of PM_{10} pollution with meteorological parameters is similar to that of $PM_{2.5}$. In Cusco, we observed a negative association between temperature and $PM_{2.5}$ concentrations, which was especially notable in 2017. This inverse relationship is consistent with Li et al. [104], suggesting high temperatures can lead to efficient vertical dispersion of pollutants. The negative relationship between wind speed and $PM_{2.5}$ and PM_{10} concentrations is consistent with findings in Barranquilla, Colombia. This negative correlation shows the importance of horizontal dispersion in reducing particulate matter concentrations [105]. Relative humidity showed a consistent negative association with $PM_{2.5}$ concentrations throughout

the three years studied in Cusco. This relationship aligns with observations in Sao Carlos, Brazil, where the highest PM_{10} concentrations occurred during dry periods characterized by reductions in rainfall and relative humidity [106]. The persistence of this negative association suggests that relative humidity plays a pivotal role in reducing particle concentrations, possibly through wet deposition mechanisms. Atmospheric pressure showed a positive association with $PM_{2.5}$ in 2018 but a negative one in 2020. This variability could be related to changes in high and low-pressure systems that affect atmospheric stability and pollutant dispersion, as Su Y. et al. [103] suggested. The complexity of this relationship underlines the need to consider interactions between multiple meteorological variables when analyzing the dynamics of atmospheric pollutants.

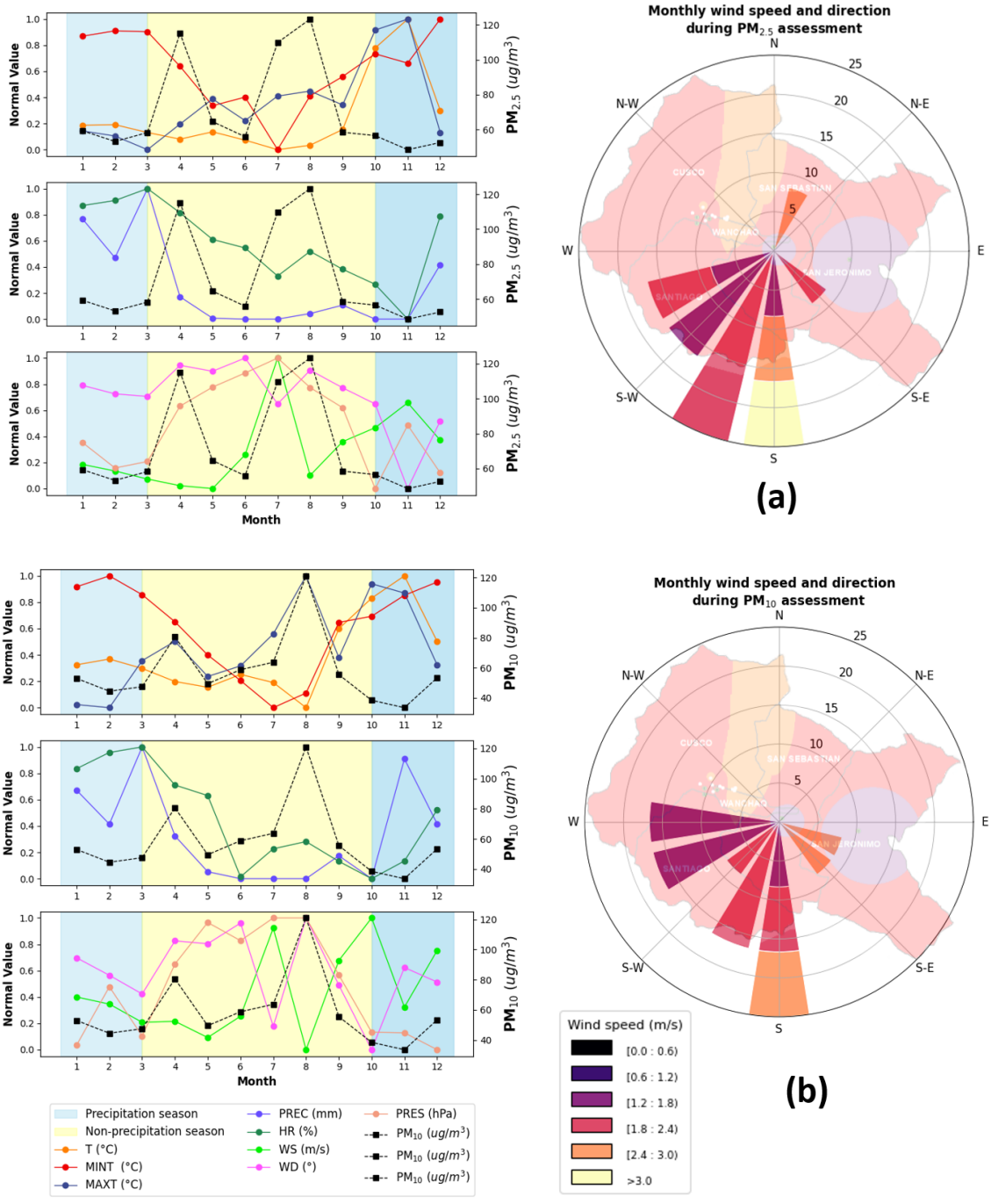


Figure 5. Monthly variation, throughout the study period, of the concentration of particulate matter and meteorological parameters: (**a**) $PM_{2.5}$, (**b**) PM_{10}.

3.2. Environmental Quality Standard and Air Quality Index

The average concentrations of $PM_{2.5}$ and PM_{10} for individual monitoring sites and districts were compared with WHO AQGs (2005 and 2021), as shown in Figure 6.

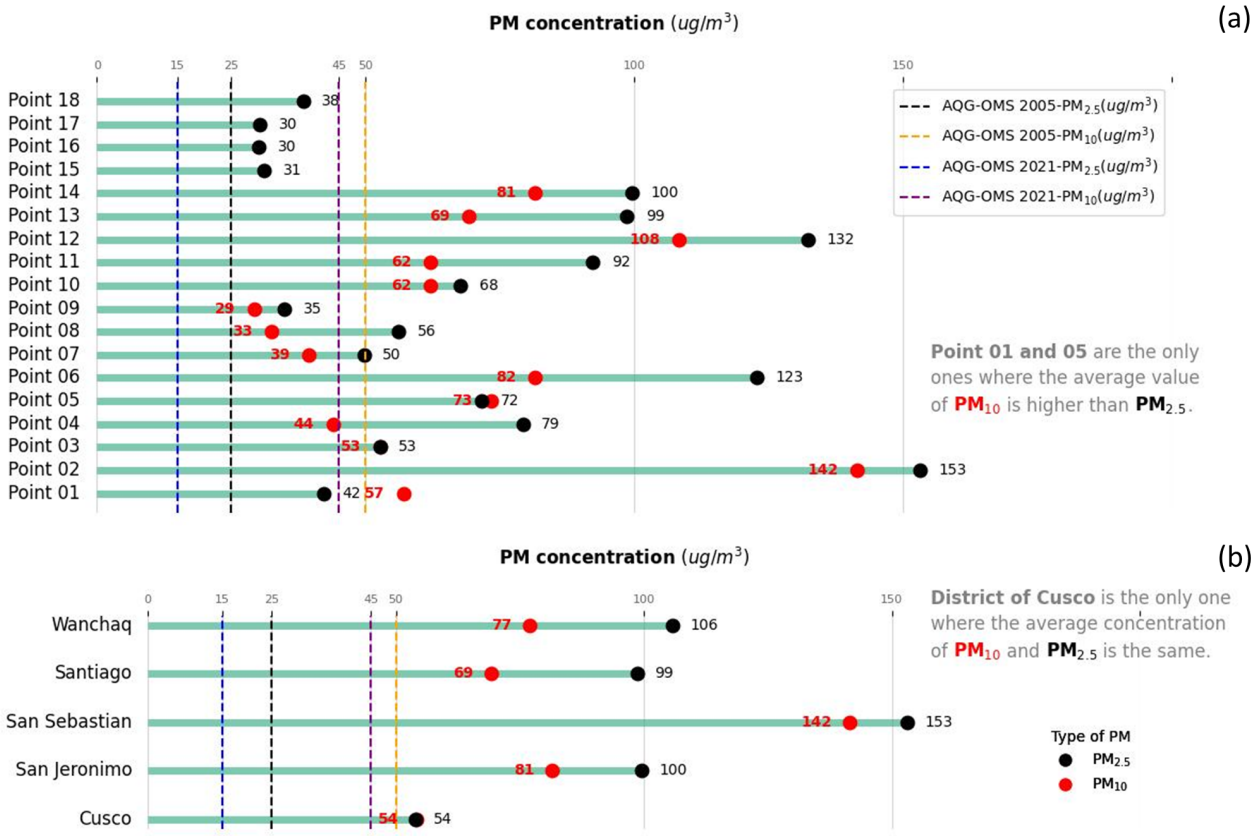


Figure 6. Average concentration of $PM_{2.5}$ and PM_{10} for (**a**) each monitoring site and (**b**) each district, compared to WHO AQG of 2005 and 2021.

Figure 6 presents two analyses, namely (a) average concentrations of $PM_{2.5}$ and PM_{10} at individual monitoring sites and (b) average concentrations by district. In panel (a), the vertical axis lists monitoring sites (site 01 to site 18), while the horizontal axis shows particulate matter concentrations in $\mu g/m^3$. Black sites represent $PM_{2.5}$ concentrations and red sites indicate PM_{10} concentrations. An unusual pattern is observed where sites 01 and 05 show higher average PM_{10} concentrations compared to $PM_{2.5}$, which is uncommon as $PM_{2.5}$ typically represents a fraction of PM_{10}. This anomaly may be attributed to specific sources of coarse particles, such as road dust or construction activities at these locations. For the remaining sites, $PM_{2.5}$ concentrations are generally higher than or equal to PM_{10}, indicating a predominance of fine particles. Site 01 exhibits the highest concentrations with 153 $\mu g/m^3$ for PM_{10} and 142 $\mu g/m^3$ for $PM_{2.5}$. Sites 05, 06, and 12 also show notably elevated levels exceeding WHO AQGs. The figure presents horizontal lines representing WHO air quality guidelines from 2005 and 2021. Most monitoring sites significantly exceed these guidelines for both $PM_{2.5}$ and PM_{10}, including the more stringent 2021 standards. Panel (b) of Figure 6 shows average $PM_{2.5}$ and PM_{10} concentrations by district. The vertical axis lists the districts: Wanchaq, Santiago, San Sebastian, San Jeronimo, and Cusco. Similar to panel (a), the horizontal axis displays average concentrations with $PM_{2.5}$ in black and PM_{10} in red. The Cusco district shows identical average concentrations for $PM_{2.5}$ and PM_{10} (54 $\mu g/m^3$). In contrast, San Sebastian and San Jeronimo record the highest average concentrations, with San Sebastian reaching 81 $\mu g/m^3$ for $PM_{2.5}$ and 100 $\mu g/m^3$ for PM_{10}, while San

Jeronimo shows 77 μg/m^3 for $PM_{2.5}$ and 106 μg/m^3 for PM_{10}. All districts exceed 2005 and 2021 WHO guidelines, indicating significant air quality concerns, although the Cusco district maintains the lowest levels among all districts. The analysis reveals significant particulate matter pollution throughout the study area, with levels substantially exceeding WHO air quality guidelines for both $PM_{2.5}$ and PM_{10}. This evidence indicates a critical air quality situation that could impact public health in these areas, emphasizing the need to identify and mitigate emission sources in key locations and districts, mainly site 01, site 05, San Sebastian, and San Jeronimo.

The Air Quality Index (AQI) analysis for $PM_{2.5}$ and PM_{10} in Cusco during 2017, 2018, and 2020 reveals a significant evolution in the city's air quality, with important implications for public health and urban environmental management. In 2017, as shown in Figure 7a, Air Quality Index (AQI) levels for $PM_{2.5}$ in Cusco were predominantly in the "Unhealthy" category (151–200), evidenced by the dark red color in most of the map. A purple zone stands out in San Sebastian and part of Wanchaq, suggesting "Very Unhealthy" levels (201–300). This situation implies significant health effects for the entire population, accentuating risks for vulnerable groups. Figure 7b, which represents PM_{10} levels in the same year, shows equally worrying conditions, with a primarily red map indicating "Unhealthy" levels and purple zones in San Sebastian, part of Wanchaq and San Jeronimo, indicating "Very Unhealthy" levels. The year 2018, illustrated in Figure 7c, showed a persistence of alarming conditions for $PM_{2.5}$. AQI levels remained in the "Unhealthy" category, with the map mostly in red. San Jeronimo and a small area between Cusco and Wanchaq showed a trend towards "Very Unhealthy" levels. Figure 7d, corresponding to PM_{10} in 2018, reveals a similar situation, with "Unhealthy" levels in general and San Jeronimo tending slightly towards "Very Unhealthy" levels. However, a slight improvement was perceived compared to 2017. A notable change was observed in 2020. Figure 7e, which shows the AQI levels for $PM_{2.5}$, shows a significant improvement, falling into the "Unhealthy for Sensitive Groups" category (101–150), represented by the uniform orange color on the map. This improvement suggests a reduction in the risk to public health, although it still indicates the presence of significant air pollution. Figure 7f, corresponding to PM_{10} in 2020, presents a similar situation, with levels in the "Unhealthy for Sensitive Groups" category, although the orange tone tending to red suggests values close to the upper limit of this category. This evolution shows an improvement in Cusco's air quality from 2017 to 2020, moving from mostly "Unhealthy " and "Very Unhealthy" levels to "Unhealthy for Sensitive Groups." However, pollution levels remain worrying and require continued attention to protect public health. Consistently, $PM_{2.5}$ levels appear more problematic than PM_{10} levels, suggesting the need to focus on controlling sources of fine particles. The significant improvement observed in 2020 could be related to the restrictions on mobility and economic activity caused by the COVID-19 pandemic. This offers a unique perspective on the potential for improving air quality under reduced anthropogenic activities. However, despite the improvements, AQI levels in 2020 remain in the "Moderate" category, indicating that health risks persist, especially for individuals sensitive to air pollution. The fluctuations observed between years suggest the influence of changes in traffic patterns or economic activities. The improvement observed in 2020 could serve as a benchmark for setting more ambitious targets in air quality management.

The Air Quality Index was calculated for both pollutants, $PM_{2.5}$ and PM_{10}. $PM_{2.5}$ was the representative pollutant due to its high AQI levels compared to PM_{10}. These $PM_{2.5}$ monitoring results in Cusco in Figure 8 reveal a worrying picture of the city's air quality. The spatial distribution of pollution levels shows significant variability among the 18 monitoring sites, spanning four categories of the EPA Air Quality Index (AQI): Moderate, Unhealthy for Sensitive Groups, Unhealthy, and Very Unhealthy. An interesting

variation in Figure 8a is observed on the National University of San Antonio Abad del Cusco (UNSAAC) campus. Sites S15 and S16 (Gate 3 and Faculty of Economics) present the lowest levels of $PM_{2.5}$, with values of 95 and 96, respectively, categorized as Moderate. This suggests that certain university campus areas enjoy relatively better air quality. However, other sites within the same campus, such as S17 (Faculty of Tourism) and S18 (Square Tricentenario), show higher levels (107 and 120), classified as Unhealthy for Sensitive Groups. This disparity within the same campus could be attributed to differences in proximity to emission sources, such as nearby traffic routes or specific activities in each area. It is particularly alarming that most monitoring sites (13 out of 18) are in the Unhealthy or Very Unhealthy categories. The most critical levels are observed in residential and public service areas. For example, site S2 in APV Paraíso de Fátima, San Sebastian, shows a value of 234 (Very Unhealthy), possibly due to its proximity to brick manufacturing industries. Similarly, San Jeronimo Health Centre (S14) presents the highest level with 246, which is extremely worrying considering that it is a healthcare facility. A notable variability is observed in the historic center, a crucial area for tourism. While Square San Blas (S9) remains in the Unhealthy for Sensitive Groups range (114), other areas such as San Francisco Square (S7 and S8), Limacpampa Square (S10), and Square Pumacchupan (S11) fall into the Unhealthy category, with values between 165 and 186. Calle Matara (S12), with a value of 212, reaches the Very Unhealthy level, possibly due to traffic congestion and the urban configuration that could hinder the dispersion of pollutants. Health centers and municipal areas also show worrying levels. The Wanchaq Health Centre (S6) and Wanchaq Municipality (S5) present values of 213 (Very Unhealthy) and 172 (Unhealthy), respectively. This is particularly alarming given that these places serve potentially vulnerable populations and are activity centers. To determine the Air Quality Index (AQI) values for $PM_{2.5}$ in each district, the value with the highest concentration of $PM_{2.5}$ within each district was considered by EPA regulations [79].

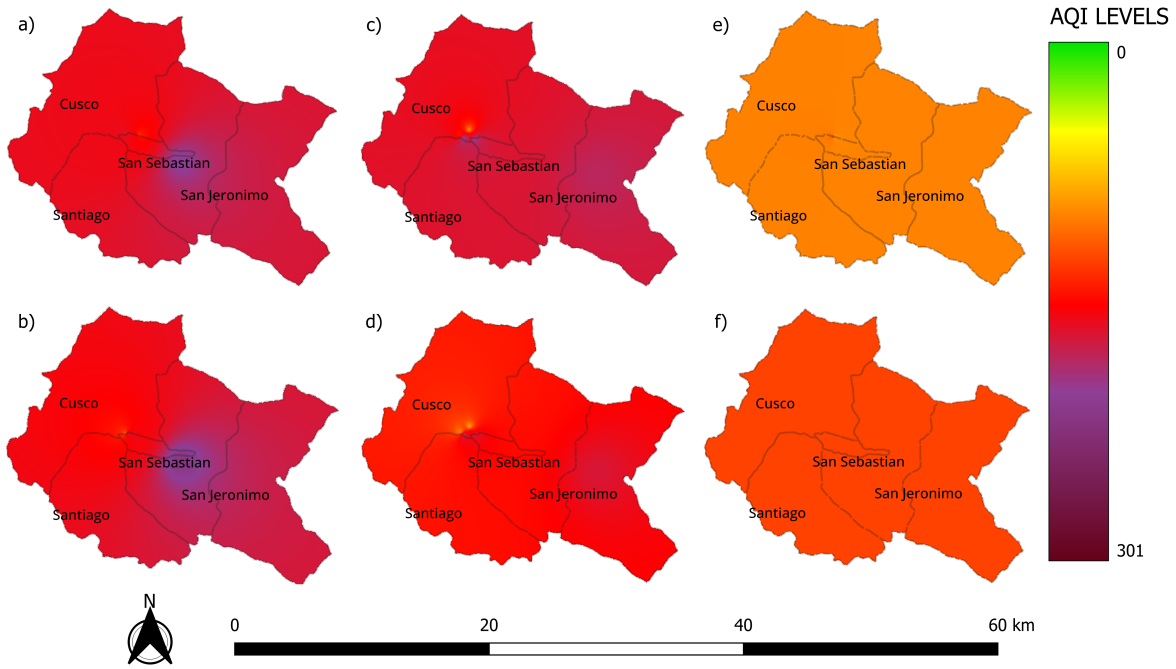


Figure 7. Heatmap of $PM_{2.5}$ and PM_{10}12 (Matara Street) also show alarming levels, wi AQI levels in the different assessment years. The subfigures show: (**a**) $PM_{2.5}$ AQI levels in 2017, (**b**) PM_{10} AQI levels in 2017, (**c**) $PM_{2.5}$ AQI levels in 2018, (**d**) PM_{10} AQI levels in 2018, (**e**) $PM_{2.5}$ AQI levels in 2020, and (**f**) PM_{10} AQI levels in 2020.

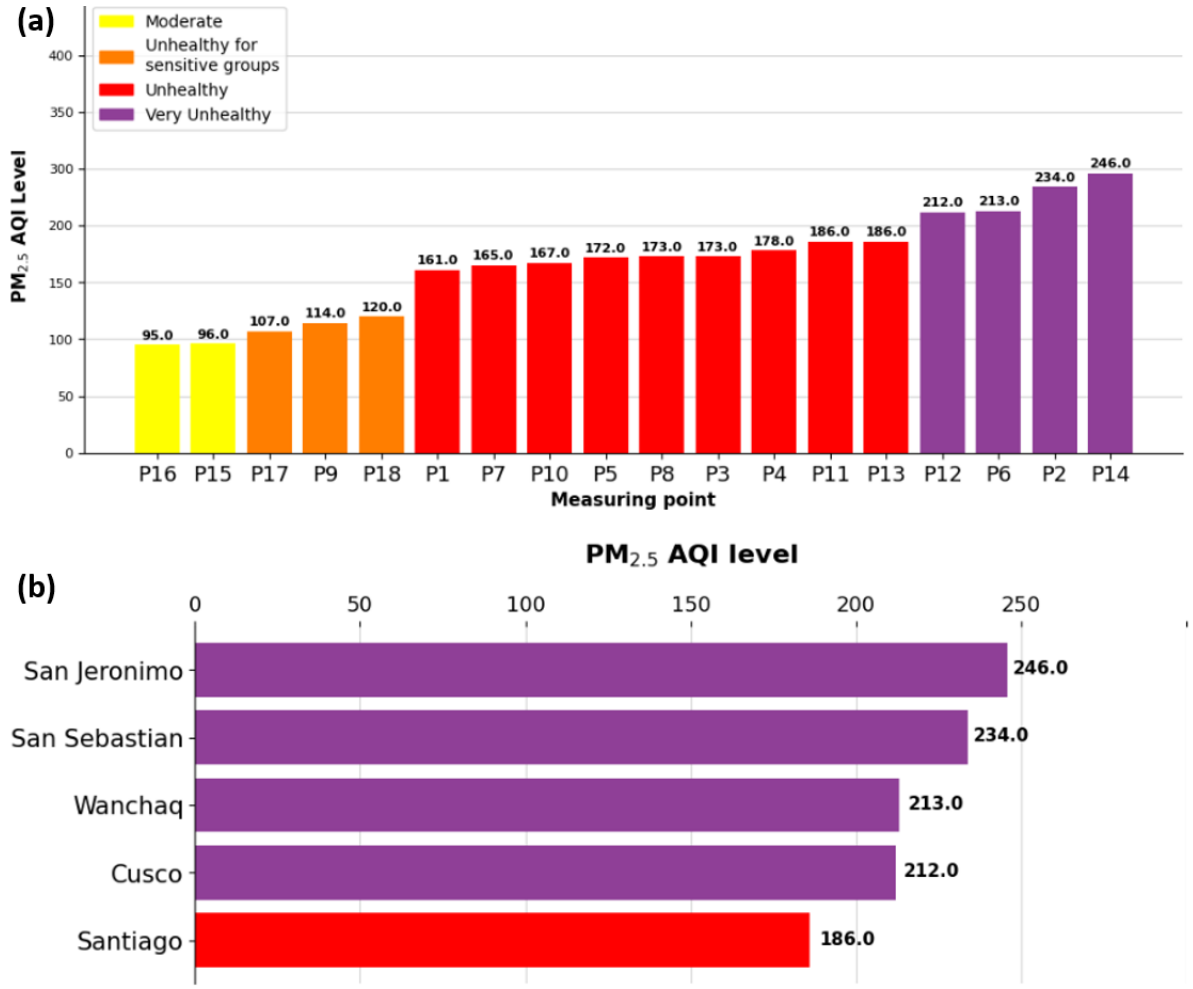


Figure 8. A bar chart of the AQI level for $PM_{2.5}$, in (**a**) each monitoring site and (**b**) each district of the city of Cusco.

The analysis of $PM_{2.5}$ distribution in the five central districts of Cusco in Figure 8b reveals a worrying picture of air quality throughout the city. All districts studied present levels classified as Unhealthy or Very Unhealthy, indicating a widespread air pollution problem. San Jeronimo is the most affected district, with an alarming AQI of 246, which places it firmly in the Very Unhealthy category. This extremely high level suggests the presence of significant emission sources in the area, possibly related to its location on one of the main access roads to the city. This could involve heavy vehicular traffic, including heavy transport. San Sebastian follows closely behind with an AQI of 234, also in the Very Unhealthy category. The similarity in levels between San Jeronimo and San Sebastian could indicate that both districts share similar characteristics in terms of pollution sources and urbanization patterns, possibly influenced by their peripheral position in the city. Wanchaq's AQI is 213, putting it in the Very Unhealthy category. This district, which houses essential administrative and service centers, has pollution levels that represent a significant health risk to residents. These levels suggest intense urban activity and traffic congestion on its main arteries. The central district of Cusco has an AQI of 212, just below Wanchaq but still in the Very Unhealthy category. This level is particularly alarming given the area's heritage character and its importance as a tourist and cultural center. The high pollution in this area could be related to the density of commercial and tourist activities, combined with an old urban layout that could hinder the dispersion of pollutants. Santiago has the lowest AQI among the districts analyzed, but its value of 186 is still worrying,

classifying it in the Unhealthy category. Although this level is relatively lower compared to the other districts, it still represents a significant risk to the population's health, especially for sensitive groups. The distribution of pollution levels suggests that the primary sources of $PM_{2.5}$ in Cusco could be related to vehicular traffic, commercial and tourist activities, and residential combustion practices. Cusco's unique topography, situated in a valley, could also play an essential role in the accumulation and distribution of pollutants. Figure 9 shows a map of the spatial distribution of pollution levels from the 18 monitoring sites, showing significant variability.

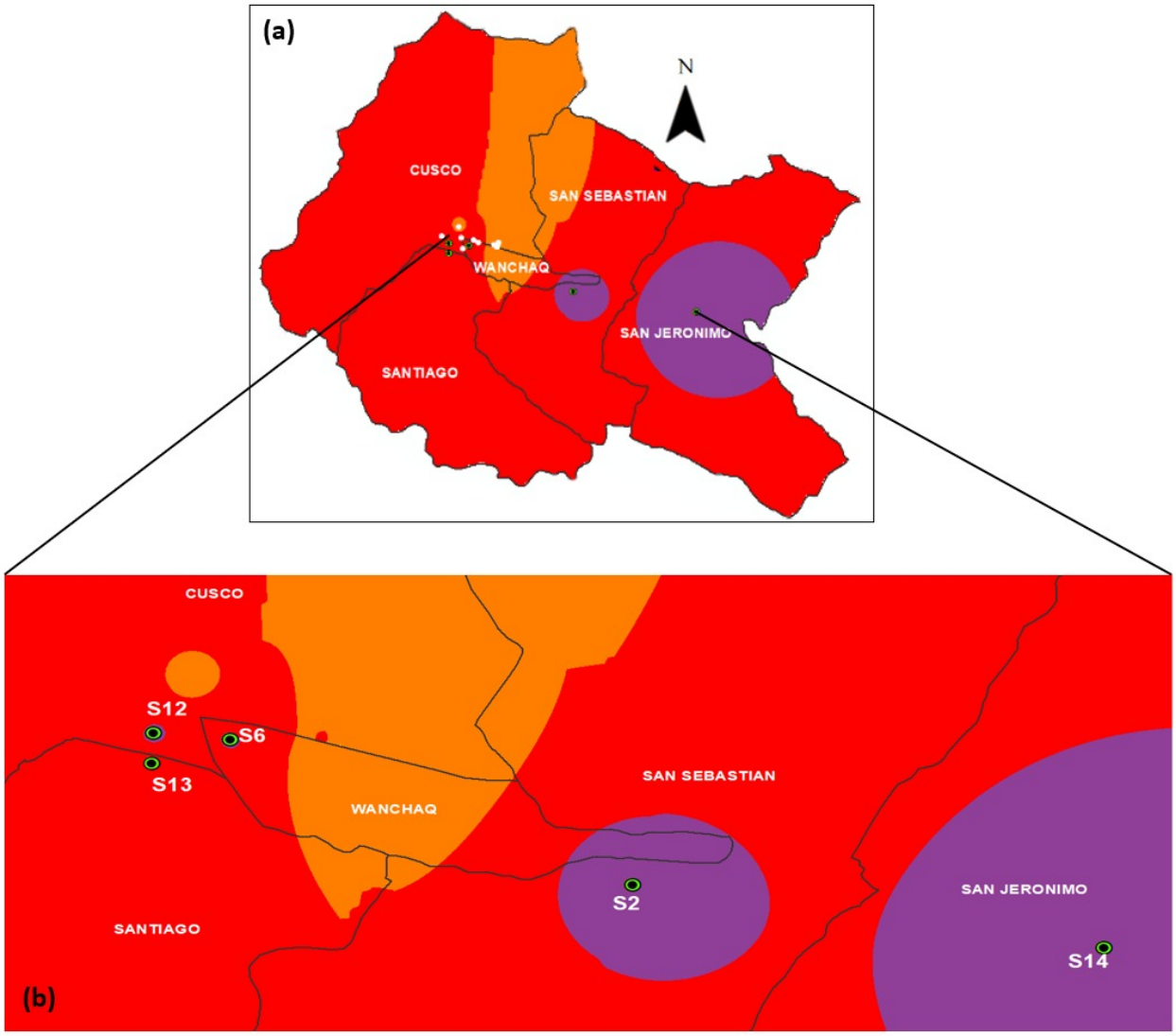


Figure 9. A heatmap on the AQI level for each monitoring site belonging to the different districts. (**a**) Map showing the districts of Cusco city: Cusco, Santiago, San Sebastian, Wanchaq, and San Jeronimo; (**b**) Detailed view of monitoring sites distribution across the districts.

The spatial distribution of pollution levels at the 18 monitoring sites and the information provided by the wind rose in Figure 5 reveal interesting patterns. In the directions where the winds predominate (North–South and Northeast–Southwest), the AQI levels are very high, reaching the red category (Figure 9a). In contrast, in Figure 9b, one of the most polluted sites has been identified in the Southeast and Northeast directions, where winds are minimal, with an AQI in the purple category, indicating even higher pollution levels. This distribution suggests that local topography and emission sources play a crucial role in the dispersion and concentration of pollutants. The results reveal a worrying air

quality situation, with $PM_{2.5}$ and PM_{10} concentrations significantly exceeding the limits set by the WHO. This scenario is not unique to Cusco but reflects a global trend in many urban areas, particularly developing countries. The marked spatial variability observed in Cusco, with PM concentrations ranging between "Moderate" and "Very Unhealthy" AQI categories, is consistent with patterns observed in other urban studies. For example, in Faisalabad, Pakistan, Zeeshan, N et al. [107] found similar variability, with $PM_{2.5}$ concentrations ranging from 55.5 $\mu g/m^3$ to over 500 $\mu g/m^3$ at different locations in the city. The temporal evolution of air quality in Cusco, with a notable improvement in 2020, is consistent with global observations during the COVID-19 pandemic. Bao and Zhang [108] showed that COVID-19-related travel restrictions reduced AQI and $PM_{2.5}$ concentrations, mediated by decreased human mobility. This phenomenon was observed in Cusco, where AQI levels went from "Unhealthy" and "Very Unhealthy" in 2017–2018 to "Unhealthy for Sensitive Groups" in 2020. The study by Benchrif et al. [102] in 21 cities around the world shows that many towns experienced significant improvements during the lockdown, moving from "moderately polluted" and "very unhealthy" categories to "slightly polluted". Our findings are comparable to those observed by Abulude et al. [109] in Owo, Nigeria, where PM values significantly exceeded the annual and 24 h mean limits of WHO standards. They also resemble those observed by Zaib et al. [110] in five provinces in northwestern China, where $PM_{2.5}$ and PM_{10} levels consistently exceeded WHO standards. However, it is important to note one significant difference: while in the study by Zaib et al. [110] the average AQI in 2018 was below the threshold value of 100 in all cities except Xinjiang, in our study, that value of 100 significantly exceeded in almost all monitoring sites, with only two exceptions. This comparison underlines the severity of the situation in Cusco, where pollution levels are consistently higher than in many other cities studied. Contrasting our findings with the study's results by Aishan, T. et al. [111] shows a less critical but still worrying situation in the oasis city of Korla, China. In their study, the air pollution indices of $PM_{2.5}$ and PM_{10} in the range of Good (0–50) to Unhealthy for Sensitive Groups (101–150) accounted for more than 90% of the total days in the year, indicating generally satisfactory air quality. However, from 2016 to 2023, 5–10% of the days reached the Hazardous category for PM_{10} at three monitoring stations. In contrast, the situation in Cusco is significantly more severe. Our results show that the majority of monitoring sites (13 out of 18) fall into the "Unhealthy" or "Very Unhealthy" categories of the AQI, with only two sites below the "Moderate" threshold. This indicates that, while in the study by Aishan et al. [111] high pollution days were the exception, in Cusco, they represent the norm. The results indicate that Cusco faces comparable and, in some cases, more severe air quality challenges than other cities. The improvement during the 2020 lockdown reveals the potential for drastic interventions to reduce pollution. It is recommended that a continuous monitoring system be implemented and district-specific mitigation strategies developed, prioritizing critical areas such as San Jeronimo and San Sebastian.

3.3. Compliance with Assumptions and Selection of Significant Variables

The assumptions mentioned in Section 2.6 were met to build the multiple linear regression models for each season and year. This research applied various techniques for each assumption. First, a correlation matrix was created between the predictors for each year of study. Based on this matrix, the predictors with the lowest correlation and the highest relationship with the target pollutant were selected. Q-Q plots of the residuals were generated, and Shapiro–Wilk tests were performed to verify the normality of the data. To comply with homoscedasticity, residual plots were constructed against the fitted values. Each hypothesis was verified for each model by season and year for both $PM_{2.5}$ and PM_{10}.

However, Figure 10 only shows the assumption plots for the best models for each PM type. Finally, the residual diagnosis for the best models built for $PM_{2.5}$ and PM_{10} is presented.

To construct the multiple linear regression models for each season and year, the assumptions mentioned in Section 2.6 were fulfilled. Multiple techniques were employed to verify each assumption. A correlation matrix was developed for each study year. Predictors with lower mutual correlation and stronger relationships with the target pollutant were selected to reduce multicollinearity. Residual normality was assessed through Q-Q plots and Kolmogorov–Smirnov tests, determining whether residuals followed a normal distribution, a fundamental requirement for model validity. Homoscedasticity was evaluated by generating residual plots against fitted values, helping identify potential non-constant variance issues that could affect prediction quality. Assumptions were exhaustively evaluated for models by season and year for both $PM_{2.5}$ and PM_{10}. However, Figure 10 presents only the results for the best models of each pollutant type. For $PM_{2.5}$, Figure 10a includes various analyses reflecting the model's predictive capacity. The predicted versus actual values plot shows reasonable performance, though dispersion around the diagonal line indicates prediction errors. Residual plots reveal no clear patterns, which is favorable, though observed variability could indicate heteroscedasticity. Residual distribution appears relatively normal, with some extreme values potentially representing outliers, but they do not significantly affect the model. The Q-Q plot confirms overall residual normality, with minor deviations at the extremes. Finally, the residuals versus predictions plot display a random distribution, indicating no evident patterns in model errors. For PM_{10}, Figure 10b presents a similar analysis. Predicted versus actual values demonstrate acceptable predictive capacity, though significant dispersion exists around the diagonal line. Residual plots reveal no evident patterns, though variability suggests potential heteroscedasticity. Residual distribution appears relatively normal, with deviations possibly linked to outliers, but these do not substantially affect the model. The Q-Q plot reaffirms residual normality, with slight deviations at extreme values. Residuals versus predictions indicate randomness in errors, though variability may again point to heteroscedasticity.

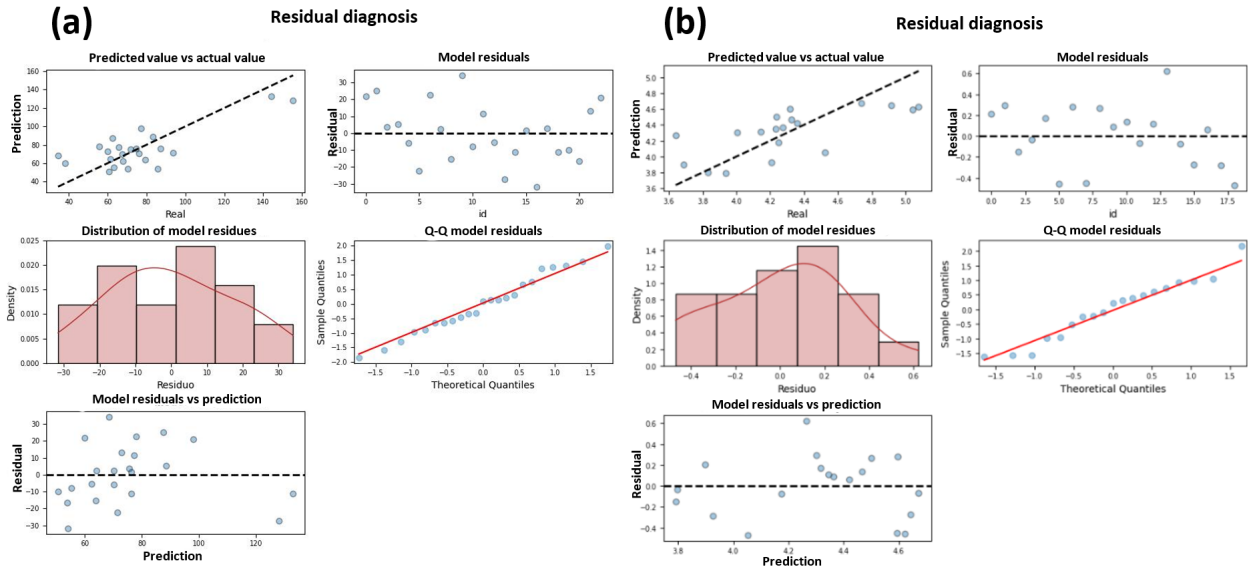


Figure 10. Residue diagnostics (**a**) Residue diagnostics for the best model built for $PM_{2.5}$; (**b**) Residue diagnostics for the best model built for PM_{10}.

3.4. MLR Models and Model Evaluation

In this study, seasonal and annual models were built. Each seasonal and annual model had two submodels, the first without transformation and the second with logarithmic

transformation. Some studies indicate a considerable improvement in their models when applying logarithmic transformation [112–114]. The results of the models built based on seasonal and annual data are shown in Table 2.

Table 2. MLR models based on seasonal and annual data.

Year	Target Variable	Season	Model	Model Equation
2017	$PM_{2.5}$	Dry	1	456.98 − 17.42*T − 3.08*HR
			2	5.63 − 0.09*Tmin − 0.02*HR
		Rainy	1	8124.56 − 11.74*PRES
			2	174.01 − 0.25*PRES
		Annual	1	365.48 − 2.43*HR − 15.21*T + 27.63*Season
			2	6.67 − 0.02*HR − 0.11*T
	PM_{10}	Dry	1	203.36 + 62.26*DL − 2.39*HR
			2	2.17 − 0.07*TMIN + 0.11*TMAX
		Rainy	1	8124.56 − 11.74*PRES
			2	3.85 + 0.49*DL
		Annual	1	99.2 − 6.23*TMIN + 57.27*DL
			2	4.79 − 0.54*Season − 0.73*DL
2018	$PM_{2.5}$	Dry	1	68.6 + 9.08*TMIN
			2	4.2 + 0.1*TMIN
		Rainy	1	207.45 − 2.16*HR
			2	10.38 − 0.06*HR − 0.26*T − 0.48*WS
		Annual	1	−7547.84 − 1.83*HR + 11.26*PRES
			2	5.23 − 0.55*Season
	PM_{10}	Dry	1	68.6 + 9.08*TMIN
			2	2 + 0.12*TMAX
		Rainy	1	207.45 − 2.16*HR
			2	1.62 + 0.11*TMAX
		Annual	1	−1241 − 22.38*Season + 5.34*TMAX
			2	2.22 − 0.4*Season + 0.12*TMAX
2020	$PM_{2.5}$	Dry	1	39524.74 − 5.6*PRES
			2	90.73 − 0.13*PRES − 0.26*DL
		Rainy	1	62.35 + 25.31*DL − 2.47*TMIN
			2	−68.12 + 0.05*TMAX + 0.1*PRES + 0.43*DL
		Annual	1	35,710.12 − 5.12*PRES
			2	94.98 − 0.13*PRES
	PM_{10}	Dry	1	39524.74 − 5.6*PRES
			2	2.27 − 0.09*TMIN − 0.05*DS − 0.17*PREC + 0.15*T
		Rainy	1	37.65 + 2.98*PREC
			2	6.03 − 0.14*T − 0.0016*WD
		Annual	1	69.93 − 3.35*DS − 0.05*WD
			2	4.27 − 0.07*DS − 0.0011*WD
FULL	$PM_{2.5}$	Dry	1	166.23 + 15.97*PREC + 5.41*DS − 6.13*T
			2	129.29 − 0.07*DS − 0.18*PRES − 0.12*T
		Rainy	1	90.43 − 12.78*WS
			2	147.41 − 0.11*WS − 0.21*PRES − 0.08*TMAX
		Annual	1	145.08 − 3.95*DS − 4.93*T
			2	48.42 − 0.06*PRES − 0.06*DS − 0.08*T
	PM_{10}	Dry	1	−77.02 + 9.51*TMAX − 4.5*T
			2	1.40 + 0.14*MAX − 0.3*DL − 0.06*TMIN
		Rainy	1	118.32 − 5.05*T
			2	5.44 − 0.12*T
		Annual	1	0.31 + 6.7*TMAX − 6.2*T
			2	3.09 + 0.11*TMAX − 0.12*T

where T: temperature; HR: relative humidity; PRES: pressure; DL: day length; TMIN: minimum temperature; TMAX: maximum temperature; WS: wind speed; DS: solar duration; PREC: precipitation; WD: wind direction.

This study analyzed various models to predict $PM_{2.5}$ and PM_{10} concentrations, considering dry seasons, rainy seasons, and annual periods. For $PM_{2.5}$, in the dry season of 2017, model 1 explained 80% of the variability and obtained an IOA of 0.74. In the rainy season of 2020, model 2 explained 98% of the variability, with an IOA of 0.49. Despite the low IOA, it is considered robust due to the inclusion of various variables. In the annual analysis

of 2020, model 2 explained 98% of the variability, but its only predictor is atmospheric pressure and an IOA of 0.44, which limits its robustness.

Regarding PM_{10}, for the dry season, considering the entire study period, model 1 explained 45% of the variability and obtained an IOA of 0.26. It is considered robust because it includes various meteorological variables. For the rainy season, also considering the entire study period, model 2 presented an R^2 of 0.16 and an IOA of 0.5. This model was selected due to the high relationship between temperature and PM_{10} concentration. The best annual model for PM_{10} was model 2 from 2018, which explained 44% of the variability and obtained an IOA of 0.52. This model is considered robust because it includes multiple predictor variables. In our study, the most robust models for $PM_{2.5}$ and PM_{10} showed different characteristics. For $PM_{2.5}$, the 2020 rainy season model (Model 2) was the most robust, explaining 98% of the variability. This model stood out for the inclusion of multiple predictor variables. On the other hand, for PM_{10}, the 2018 annual model (Model 2) proved to be the most robust, explaining 44% of the variability with an IOA of 0.52. It is important to note that although some models in our study showed superior metrics (as seen in Table 3), they were not selected due to their lower robustness by not including a diversity of predictors. This decision was made because a more complex model incorporating multiple predictor variables may be more generalizable and applicable to different environmental conditions. It is also worth noting that the best models used a logarithmic transformation in both cases. This technique has proven to be especially effective in capturing the nonlinear relationships between pollutants and meteorological variables, consistent with previous studies that have reported significant improvements when applying this transformation [115–117]. Our $PM_{2.5}$ findings agree with those reported by Zhao et al. [68] in Beijing, China, who also found better performance in seasonal MLR models than annual ones. In their study, in addition to meteorological data, they used pollutants such as SO_2, NO_2, CO, and O_3 as predictors. Their R^2 and RMSE indicators revealed high suitability for spring and winter ($R^2 > 0.85$), while for summer, it was low ($R^2 = 0.761$). Except for summer, the results and prediction validity for the other three seasons were better than in the annual data. However, our model presented a relatively low IOA (0.49), suggesting that, despite its high explanatory capacity, there could be room for improvement in terms of accuracy. Regarding PM_{10}, our results are comparable to those obtained by Pyae and Kallawicha [118], who managed to explain 46% of the variance in their annual model. In their study, the model for annual $PM_{2.5}$ explained 60% of its variance, while their winter seasonal models showed the highest performance for both $PM_{2.5}$ and PM_{10}, with 30% and 29% variance explanation, respectively. In contrast, our seasonal models for PM_{10} showed inferior performance, with the best model explaining only 45% of the dry season variability. Ke et al. [71] achieved remarkable results using a combination of models. Their approach explained 79% of the variance for $PM_{2.5}$ and 76% for PM_{10}. For $PM_{2.5}$, they obtained an RMSE of 18.68, a MAPE of 45.14%, and an IA of 0.88. In the case of PM_{10}, the values were 27.32, 38.67%, and 0.85 for RMSE, MAPE, and IA, respectively. These results significantly exceed our study's results, especially for PM_{10}. The effectiveness of these advanced models suggests that incorporating more sophisticated machine learning techniques could substantially improve the predictive capacity of air quality models, opening new avenues for future research in this field. For their part, Galán-Madruga et al. [119] developed a high-performance model for $PM_{2.5}$ using a careful selection of predictor variables. These included precipitation, temperature, wind direction and speed, mean sea level pressure, and planetary boundary layer height. Their results were particularly favorable, with RMSE values of 1.8, MAE of 3.24, and MAPE of 20.60%. These findings show the importance of meticulously selecting predictor variables in air quality modeling. In particular, the inclusion of parameters such as planetary boundary

layer height is shown to have an impact on improving model performance, suggesting that the consideration of specific atmospheric variables can significantly increase the accuracy of PM predictions. In the study by Raju L. et al. [120] in Chennai, they developed different models, such as linear and nonlinear regression models, and machine learning models, such as random forest (RF), for $PM_{2.5}$ estimation. The RF model particularly stood out, explaining approximately 53.14% of the variability in $PM_{2.5}$ concentrations, with an R^2 of 0.53 and an RMSE of 15.89 $\mu g/m^3$. When comparing these findings with our results, the good performance of our best model for $PM_{2.5}$ is evident, which managed to explain 98% of the variability during the 2020 rainy season. This significant difference in the explanatory power of the models could be attributed to several factors, including the specific characteristics of each study environment, the nature and quality of the available data, and the climatic and topographical particularities of each region. Nevertheless, it is essential to recognize the robustness and effectiveness of the random forest model used by Raju et al. [120] in their specific context. For future research, exploring more advanced machine learning techniques is recommended. Likewise, it would be beneficial to consider including additional atmospheric variables, such as the height of the planetary boundary layer, following the approach of Galán-Madruga et al. [119]. Investigating the applicability of combined methods could help better capture seasonal variability. These improvements could lead to more robust and accurate models adapted to the unique conditions of Cusco and provide more effective tools for air quality management in the region. Figure 11 compares observed and predicted values for particulate matter concentrations by our multiple linear regression model. Panel (a) shows the results for $PM_{2.5}$, while panel (b) presents the data for PM_{10}. Due to the continuity of measured data, it is observed that the values predicted by the model are different from what is expected. However, this visual representation supports the first model for predicting $PM_{2.5}$ and PM_{10} concentrations in Cusco. It is expected that subsequent researchers will use other models to improve the prediction performance.

Table 3. Performance evaluation metrics for each model built.

Year	Target Variable	Season	Model	R^2	RMSE	NMSE	MAE	MAPE (%)	IOA	CV (%)
2017	$PM_{2.5}$	Dry	1	0.8	12.69	2	12.53	19	0.74	20.69
			2	0.8	13.37	2.43	11.27	18.95	0.71	21.83
		Rainy	1	0.24	17.38	5.76	13.33	16.22	0.23	7.68
			2	0.3	19.74	7.43	15.04	18.26	0.2	10.1
		Annual	1	0.59	26.02	0.25	22.4	40.59	0.89	33.25
			2	0.39	30.2	0.34	24.49	37.31	0.84	31.48
	PM_{10}	Dry	1	0.58	13.95	2.35	12.81	16.22	0.65	20.08
			2	0.49	5.97	0.33	5.33	8.46	0.92	17.33
		Rainy	1	0.24	17.38	5.76	12.3	16.22	0.23	7.68
			2	0.46	12.46	87.75	12.58	54.82	0.18	0.5
		Annual	1	0.49	32.75	0.56	24.49	28.18	0.39	18.73
			2	0.46	34.22	1.02	22.53	25.19	0.22	7.65
2018	$PM_{2.5}$	Dry	1	0.53	39.5	1.44	34.41	29.54	0.39	17.34
			2	0.55	43.47	1.74	38.41	33.39	0.49	20.88
		Rainy	1	0.17	37.89	0.97	34.9	68.01	0.34	16.42
			2	0.35	42.45	1.22	40.08	90.87	0.49	23.8
		Annual	1	0.34	41.46	1.31	31.89	60.68	0.42	28.67
			2	0.315	33.92	1.43	27.3	46.87	0.49	27.73
	PM_{10}	Dry	1	0.53	39.5	1.44	34.41	29.54	0.39	17.34
			2	0.13	26.3	1.91	23.96	37.1	0.41	13.5
		Rainy	1	0.17	37.89	0.97	34.9	68.01	0.34	16.42
			2	0.15	27.54	1.12	19.81	28.59	0.55	15.83
		Annual	1	0.38	29.72	0.89	23.56	31.69	0.51	18.05
			2	0.44	31.23	0.98	24	39.79	0.52	20.24

Table 3. *Cont.*

Year	Target Variable	Season	Model	R^2	RMSE	NMSE	MAE	MAPE (%)	IOA	CV (%)
2020	$PM_{2.5}$	Dry	1	0.35	9	1.04	7.65	29.21	0.75	19.77
			2	0.46	10.2	1.34	9.09	34.13	0.61	22.3
		Rainy	1	0.88	18.35	0.81	18.19	−74.13	0.36	5.57
			2	0.98	17.02	0.69	17.01	65.83	0.49	9.18
		Annual	1	0.32	16.27	0.95	12.96	51.34	0.47	15.77
			2	0.98	16.14	0.95	12.34	47.12	0.44	16.59
	PM_{10}	Dry	1	0.35	9	1.04	7.65	29.21	0.75	19.77
			2	0.69	11.47	0.75	11.2	60.1	0.75	31.08
		Rainy	1	0.21	21.01	7.03	14.22	21.62	0.14	19.29
			2	0.69	19.65	6.15	19.08	47.44	0.35	26.68
		Annual	1	0.41	27.74	1.92	25.63	125.22	0.37	20.4
			2	0.4	27.36	1.82	25.11	124.64	0.34	19.63
FULL	$PM_{2.5}$	Dry	1	0.38	41.1	0.72	35.73	66.75	0.55	22.07
			2	0.53	44.44	0.84	35.55	52.98	0.63	39.29
		Rainy	1	0.08	49.9	1.06	42.73	85.52	0.15	9.21
			2	0.3	52.19	1.16	41.24	63.04	0.45	40.19
		Annual	1	0.15	32.52	0.7	26.8	53.45	0.29	23.88
			2	0.21	34.54	0.79	25.39	41.45	0.56	25.03
	PM_{10}	Dry	1	0.45	35.97	1.46	28.43	41.62	0.26	16.89
			2	0.5	43.36	2.23	34.64	47.18	0.27	19.47
		Rainy	1	0.13	18.6	0.91	17.13	42.31	0.49	10.98
			2	0.16	18.9	0.87	16.55	39.11	0.51	14.27
		Annual	1	0.31	20.15	0.87	17.42	31.46	0.63	23.91
			2	0.34	21.91	0.95	16.93	29.58	0.6	24.81

where R^2: Coefficient of determination; RMSE: Root Mean Square Error; NMSE: Normalized Mean Square Error; MAE: Mean Absolute Error; MAPE: Mean Absolute Percentage Error; IOA: Index of Agreement; CV: Coefficient of Variation.

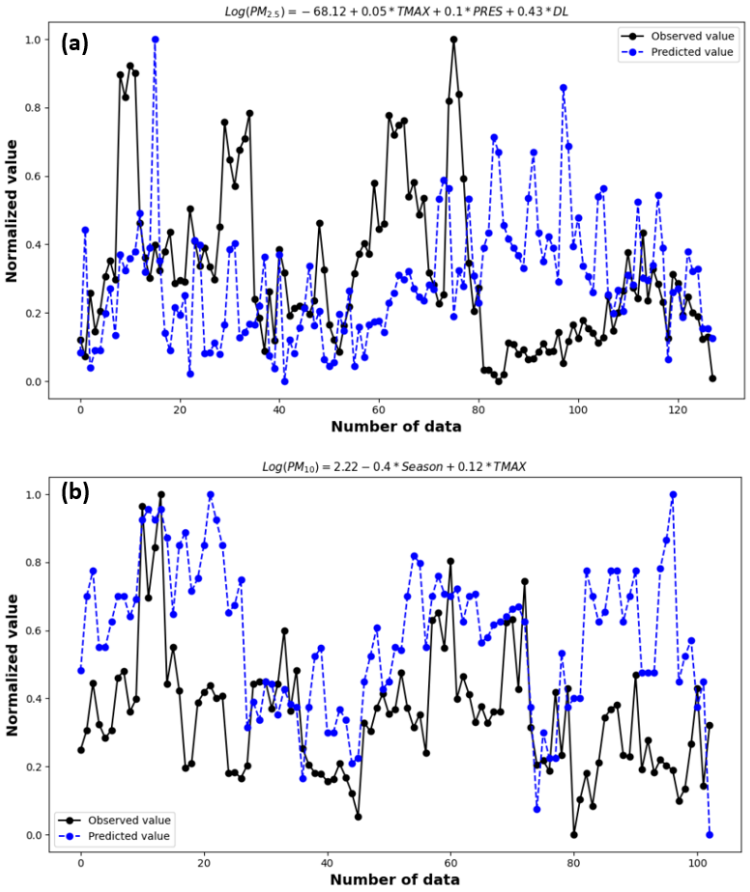


Figure 11. Observed and predicted values (**a**) $PM_{2.5}$ (**b**) PM_{10}.

4. Conclusions

This study presents the first comprehensive assessment of particulate matter ($PM_{2.5}$ and PM_{10}) contamination in the city of Cusco, revealing critical air pollution patterns that significantly exceed international standards. The temporal analysis demonstrated elevated particulate matter concentrations, with $PM_{2.5}$ levels reaching 77.46 $\mu g/m^3$ in 2017 and 82.01 $\mu g/m^3$ in 2018, showing a notable reduction to 41.10 $\mu g/m^3$ in 2020. PM_{10} concentrations followed a similar trend, with values of 72.35 $\mu g/m^3$ in 2017, 65.93 $\mu g/m^3$ in 2018, and 45 $\mu g/m^3$ in 2020. Spatial distribution identified San Jerónimo and San Sebastián as the most affected districts. Air Quality Index (AQI) values of 246 and 234, respectively, are classified as "Very Unhealthy" and represent a significant risk to public health and cultural heritage preservation. COVID-19 mobility restrictions in 2020 resulted in a substantial reduction in air pollution levels, with decreases of 46.94% in $PM_{2.5}$ and 37.72% in PM_{10} compared to previous years. These results, consistent with observed global trends, demonstrate the substantial influence urban mobility regulations can exert on air quality. The development of multiple linear regression (MLR) predictive models yielded varying results. The most robust model, corresponding to $PM_{2.5}$ during the 2020 rainy season, achieved an explanatory capacity of 98%, surpassing similar models' performance in other cities. For PM_{10}, the 2018 annual model explained 44% of variability, suggesting the need to explore more sophisticated modeling approaches. Applying logarithmic transformations in prediction models significantly improved their performance, evidencing the nonlinear nature of interactions between atmospheric pollutants and meteorological variables, a fundamental aspect for future regional research. These findings support the urgent need to implement zone-specific control measures to improve air quality in Cusco. Establishing a continuous monitoring system and implementing more advanced modeling techniques incorporating additional predictor variables is recommended, thus enabling more precise and effective long-term air quality management.

Supplementary Materials: The following supporting information can be downloaded at: https://www.mdpi.com/article/10.3390/su17020394/s1.

Author Contributions: Conceptualization, J.W., A.O., R.I., R.C. and M.A.; methodology, J.W., A.O., B.W., V.C., J.O., Y.Q., V.J., R.I., R.C. and M.A.; software, B.W., A.Z. and I.M.; validation, B.W., A.Z., I.M., D.C., R.S., M.M.-D., G.W., R.T., E.U., W.C. and J.R.; visualization, J.W., B.W., A.Z. and I.M.; project administration, J.W., B.W., M.M.Z.-P., R.I., R.C. and M.A.; data curation, B.W., A.Z., I.M., D.C., R.S., M.M.-D., G.W., R.T., E.U., W.C. and J.R.; investigation, J.W., A.O., B.W., A.Z., I.M., M.M.Z.-P., D.C., R.S., J.V., M.M.-D., R.I., G.W., R.T., E.U., W.C., R.C., J.R. and M.A.; Formal analysis, Resources, Supervision, Writing—review and editing, all authors; writing—original draft preparation, J.W., B.W., A.Z. and I.M.; funding acquisition, J.W. All authors have read and agreed to the published version of the manuscript.

Funding: This research received no external funding.

Institutional Review Board Statement: Not applicable.

Informed Consent Statement: Not applicable.

Data Availability Statement: The original contributions presented in the study are included in the article, which focuses on the models and evaluations. Further inquiries can be directed to the corresponding authors.

Acknowledgments: The authors would like to thank the Center for Energy and Atmosphere Research (CIEA-UNSAAC) members, as well as the security guards, students, and teachers who collaborated on the project to evaluate pollutants in Cusco. They extend their gratitude to the Faculty of Chemical, Physical, and Mathematical Sciences, the National University of San Antonio Abad del Cusco, and all those who contributed to the development of this article over years of measurements.

Conflicts of Interest: The authors declare no conflicts of interest.

References

1. Zalakeviciute, R.; Bastidas, M.; Buenaño, A.; Rybarczyk, Y. A traffic-based method to predict and map urban air quality. *Appl. Sci.* **2020**, *10*, 2035. [CrossRef]
2. Luo, G.; Zhang, L.; Hu, X.; Qiu, R. Quantifying public health benefits of $PM_{2.5}$ reduction and spatial distribution analysis in China. *Sci. Total Environ.* **2020**, *719*, 137445. [CrossRef] [PubMed]
3. Carreño, G.; López-Cortés, X.A.; Marchant, C. Machine learning models to predict critical episodes of environmental pollution for $PM_{2.5}$ and PM_{10} in Talca, Chile. *Mathematics* **2022**, *10*, 373. [CrossRef]
4. Power, A.L.; Tennant, R.K.; Stewart, A.G.; Gosden, C.; Worsley, A.T.; Jones, R.; Love, J. The evolution of atmospheric particulate matter in an urban landscape since the Industrial Revolution. *Sci. Rep.* **2023**, *13*, 8964. [CrossRef] [PubMed]
5. Chen, H.; Deng, G.; Liu, Y. Monitoring the influence of industrialization and urbanization on spatiotemporal variations of AQI and $PM_{2.5}$ in three provinces, China. *Atmosphere* **2022**, *13*, 1377. [CrossRef]
6. Bilal, M.; Nichol, J.E.; Nazeer, M.; Shi, Y.; Wang, L.; Kumar, K.R.; Ho, H.C.; Mazhar, U.; Bleiweiss, M.P.; Qiu, Z.; et al. Characteristics of fine particulate matter ($PM_{2.5}$) over urban, suburban, and rural areas of Hong Kong. *Atmosphere* **2019**, *10*, 496. [CrossRef]
7. Wang, Q.; Kwan, M.-P.; Zhou, K.; Fan, J.; Wang, Y.; Zhan, D. The impacts of urbanization on fine particulate matter ($PM_{2.5}$) concentrations: Empirical evidence from 135 countries worldwide. *Environ. Pollut.* **2019**, *247*, 989–998. [CrossRef] [PubMed]
8. Han, L.; Zhou, W.; Pickett, S.T.A.; Li, W.; Li, L. An optimum city size? The scaling relationship for urban population and fine particulate ($PM_{2.5}$) concentration. *Environ. Pollut.* **2016**, *208*, 96–101. [CrossRef]
9. Yang, F.; Xu, Q.; Li, K.; Yuen, K.F.; Shi, W. The inhibition effect of bank credits on $PM_{2.5}$ concentrations: Spatial evidence from high-polluting firms in China. *Environ. Pollut.* **2022**, *308*, 119639. [CrossRef] [PubMed]
10. Zhao, H.; Guo, S.; Zhao, H. Quantifying the impacts of economic progress, economic structure, urbanization process, and number of vehicles on $PM_{2.5}$ concentration: A provincial panel data model analysis of China. *Int. J. Environ. Res. Public Health* **2019**, *16*, 2926–2926. [CrossRef] [PubMed]
11. Wang, L.; Zhang, H.; Mao, L.; Li, S.; Wu, H. Assessing spatiotemporal characteristics of urban $PM_{2.5}$ using fractal dimensions and wavelet analysis. *Math. Probl. Eng.* **2020**, *2020*, 8091515. [CrossRef]
12. Pope, C.A., III; Coleman, N.; Pond, Z.A.; Burnett, R.T. Fine particulate air pollution and human mortality: 25+ years of cohort studies. *Environ. Res.* **2020**, *183*, 108924. [CrossRef] [PubMed]
13. Liu, M.; Huang, Y.; Jin, Z.; Ma, Z.; Liu, X.; Zhang, B.; Liu, Y.; Yu, Y.; Wang, J.; Bi, J.; et al. The nexus between urbanization and $PM_{2.5}$ related mortality in China. *Environ. Pollut.* **2017**, *227*, 15–23. [CrossRef] [PubMed]
14. Zhang, S.; Routledge, M.N. The contribution of $PM_{2.5}$ to cardiovascular disease in China. *Environ. Sci. Pollut. Res.* **2020**, *27*, 37502–37513. [CrossRef] [PubMed]
15. Requia, W.J.; Adams, M.D.; Arain, A.; Papatheodorou, S.; Koutrakis, P.; Mahmoud, M. Global association of air pollution and cardiorespiratory diseases: A systematic review, meta-analysis, and investigation of modifier variables. *Am. J. Public Health* **2018**, *108*, S123–S130. [CrossRef]
16. Yuan, S.; Wang, J.; Jiang, Q.; He, Z.; Huang, Y.; Li, Z.; Cai, L.; Cao, S. Long-term exposure to $PM_{2.5}$ and stroke: A systematic review and meta-analysis of cohort studies. *Environ. Res.* **2019**, *177*, 108587. [CrossRef] [PubMed]
17. Maji, K.J.; Dikshit, A.K.; Arora, M.; Deshpande, A. Estimating premature mortality attributable to $PM_{2.5}$ exposure and benefit of air pollution control policies in China for 2020. *Sci. Total Environ.* **2018**, *612*, 683–693. [CrossRef] [PubMed]
18. Wu, W.; Wu, G.; Wei, J.; Lawrence, W.R.; Deng, X.; Zhang, Y.; Chen, S.; Wang, Y.; Lin, X.; Chen, D.; et al. Potential causal links and mediation pathway between urban greenness and lung cancer mortality: Result from a large cohort (2009 to 2020). *Sustain. Cities Soc.* **2024**, *101*, 105079. [CrossRef]
19. Miller, L.; Xu, X. Ambient $PM_{2.5}$ human health effects—findings in China and research directions. *Atmosphere* **2018**, *9*, 424. [CrossRef]
20. Shi, Y.; Zhu, Y.; Gong, S.; Pan, J.; Zang, S.; Wang, W.; Li, Z.; Matsunaga, T.; Yamaguchi, Y.; Bai, Y. $PM_{2.5}$-related premature deaths and potential health benefits of controlled air quality in 34 provincial cities of China during 2001–2017. *Environ. Impact Assess. Rev.* **2022**, *97*, 106883. [CrossRef]
21. Wang, F.; Qiu, X.; Cao, J.; Peng, L.; Zhang, N.; Yan, Y.; Li, R. Policy-driven changes in the health risk of $PM_{2.5}$ and O3 exposure in China during 2013–2018. *Sci. Total Environ.* **2021**, *757*, 143775. [CrossRef]
22. Anenberg, S.C.; Horowitz, L.W.; Tong, D.Q.; West, J.J. An estimate of the global burden of anthropogenic ozone and fine particulate matter on premature human mortality using atmospheric modeling. *Environ. Health Perspect.* **2010**, *118*, 1189–1195. [CrossRef] [PubMed]
23. Meng, J.; Liu, J.; Fan, S.; Kang, C.; Yi, K.; Cheng, Y.; Shen, X.; Tao, S. Potential health benefits of controlling dust emissions in Beijing. *Environ. Pollut.* **2016**, *213*, 850–859. [CrossRef]

24. Pope, C.A., III; Burnett, R.T.; Thun, M.J.; Calle, E.E.; Krewski, D.; Ito, K.; Thurston, G.D. Lung Cancer, Cardiopulmonary Mortality, and Long-term Exposure to Fine Particulate Air Pollution. *JAMA* **2002**, *287*, 1132–1141. [CrossRef]
25. Fuller, R.; Landrigan, P.J.; Balakrishnan, K.; Bathan, G.; Bose-O'Reilly, S.; Brauer, M.; Caravanos, J.; Chiles, T.; Cohen, A.; Corra, L.; Cropper, M. Pollution and health: A progress update. *Lancet Planet Health* **2022**, *6*, e535–e547. [CrossRef] [PubMed]
26. Li, T.; Yu, Y.; Sun, Z.; Duan, J. A comprehensive understanding of ambient particulate matter and its components on the adverse health effects based from epidemiological and laboratory evidence. *Part. Fibre Toxicol.* **2022**, *19*, 67. [CrossRef]
27. Pozzer, A.; Tsimpidi, A.P.; Karydis, V.A.; deMeij, A.; Lelieveld, J. Impact of agricultural emission reductions on fine-particulate matter and public health. *Atmos. Chem. Phys.* **2017**, *17*, 12813–12826. [CrossRef]
28. Liu, J.; Kiesewetter, G.; Klimont, Z.; Cofala, J.; Heyes, C.; Schöpp, W.; Zhu, T.; Cao, G.; Sanabria, A.G.; Sander, R.; et al. Mitigation pathways of air pollution from residential emissions in the Beijing-Tianjin-Hebei region in China. *Environ. Int.* **2019**, *125*, 236–244. [CrossRef]
29. Malakootian, M.; Mohammadi, A. Estimating health impact of exposure to $PM_{2.5}$, NO2 and O-3 using AIRQ plus model in Kerman, Iran. *Environ. Eng. Manag. J.* **2020**, *19*, 1317–1323. Available online: https://eemj.eu/index.php/EEMJ/article/view/4150 (accessed on 24 February 2024).
30. Zhang, Y.; Liu, D.; Liu, Z. Fine particulate matter ($PM_{2.5}$) and chronic kidney disease. *Rev. Environ. Contam. Toxicol.* **2021**, *254*, 183–215. [CrossRef] [PubMed]
31. Diao, B.; Ding, L.; Zhang, Q.; Na, J.; Cheng, J. Impact of urbanization on $PM_{2.5}$-related health and economic loss in China 338 cities. *Int. J. Environ. Res. Public Health* **2020**, *17*, 990. [CrossRef] [PubMed]
32. Marlier, M.E.; Brenner, K.I.; Liu, J.C.; Mickley, L.J.; Raby, S.; James, E.; Ahmadov, R.; Riden, H. Exposure of agricultural workers in California to wildfire smoke under past and future climate conditions. *Environ. Res. Lett.* **2022**, *17*, 094045. [CrossRef]
33. Hoffman, S.; Jasiński, R. The use of multilayer perceptrons to model $PM_{2.5}$ concentrations at air monitoring stations in Poland. *Atmosphere* **2023**, *14*, 96. [CrossRef]
34. Lelieveld, J.; Evans, J.S.; Fnais, M.; Giannadaki, D.; Pozzer, A. The contribution of outdoor air pollution sources to premature mortality on a global scale. *Nature* **2015**, *525*, 367–371. [CrossRef]
35. Renard, J.-B.; Surcin, J.; Annesi-Maesano, I.; Poincelet, E. Temporal evolution of $PM_{2.5}$ levels and COVID-19 mortality in Europe for the 2020–2022 period. *Atmosphere* **2023**, *14*, 1222. [CrossRef]
36. EPA. Particulate Matter (PM) Basics. Available online: https://www.epa.gov/pm-pollution/particulate-matter-pm-basics (accessed on 4 December 2024).
37. Kim, D.-Y.; Jin, D.-Y.; Suk, H.-I. Spatiotemporal graph neural networks for predicting mid-to-long-term $PM_{2.5}$ concentrations. *J. Clean. Prod.* **2023**, *425*, 138880. [CrossRef]
38. Isaifan, R.J. Air pollution burden of disease over highly populated states in the Middle East. *Front. Public Health* **2023**, *10*, 1002707. [CrossRef]
39. Aguilera, R.; Gershunov, A.; Ilango, S.D.; Guzman-Morales, J.; Benmarhnia, T. Santa Ana winds of southern California impact $PM_{2.5}$ with and without smoke from wildfires. *GeoHealth* **2020**, *4*, e2019GH000225. [CrossRef] [PubMed]
40. Zhao, J.; Li, M.; Wang, Z.; Chen, J.; Zhao, J.; Xu, Y.; Wei, X.; Wang, J.; Xie, J. Role of $PM_{2.5}$ in the development and progression of COPD and its mechanisms. *Respir. Res.* **2019**, *20*, 1081. [CrossRef]
41. Gan, W.Q.; FitzGerald, J.M.; Carlsten, C.; Sadatsafavi, M.; Brauer, M. Associations of ambient air pollution with chronic obstructive pulmonary disease hospitalization and mortality. *Am. J. Respir. Crit. Care Med.* **2013**, *187*, 721–727. [CrossRef] [PubMed]
42. Lin, H.; Guo, Y.; Zheng, Y.; Di, Q.; Liu, T.; Xiao, J.; Li, X.; Zeng, W.; Cummings-Vaughn, L.A.; Howard, S.W.; et al. Long-term effects of ambient $PM_{2.5}$ on hypertension and blood pressure and attributable risk among older Chinese adults. *Hypertension* **2017**, *69*, 806–812. [CrossRef]
43. Juarez, P.D.; Tabatabai, M.; Burciaga Valdez, R.; Hood, D.B.; Im, W.; Mouton, C.; Colen, C.; Al-Hamdan, M.Z.; Matthews-Juarez, P.; Lichtveld, M.Y.; et al. The effects of social, personal, and behavioral risk factors and $PM_{2.5}$ on cardio-metabolic disparities in a cohort of community health center patients. *Int. J. Environ. Res. Public Health* **2020**, *17*, 3561. [CrossRef] [PubMed]
44. Liu, C.W.; Lee, T.L.; Chen, Y.C.; Liang, C.J.; Wang, S.H.; Lue, J.H.; Tsai, J.S.; Lee, S.W.; Chen, S.H.; Yang, Y.F.; et al. $PM_{2.5}$-induced oxidative stress increases intercellular adhesion molecule-1 expression in lung epithelial cells through the IL-6/AKT/STAT3/NF-κB-dependent pathway. *Part. Fibre Toxicol.* **2018**, *15*, 240. [CrossRef]
45. Sørensen, M.; Daneshvar, B.; Hansen, M.; Dragsted, L.O.; Hertel, O.; Knudsen, L.; Loft, S. Personal $PM_{2.5}$ exposure and markers of oxidative stress in blood. *Environ. Health Perspect.* **2003**, *111*, 161–166. [CrossRef]
46. World Health Organization. WHO Global Air Quality Guidelines: Particulate Matter ($PM_{2.5}$ and PM_{10}), Ozone, Nitrogen Dioxide, Sulfur Dioxide and Carbon Monoxide. WHO. 2021. Available online: https://www.who.int/publications/i/item/9789240034228 (accessed on 4 December 2024).
47. World Health Organization. Air Quality Guidelines Global Update 2005. WHO. 2006. Available online: https://www.who.int/publications/i/item/WHO-SDE-PHE-OEH-06.02 (accessed on 4 December 2024).

48. do Nascimento, C.M.; deOliveira, S.A.; Santana, O.A.; Carvalho, H. Changes in air pollution due to COVID-19 lockdowns in 2020: Limited effect on NO2, $PM_{2.5}$, and PM_{10} annual means compared to the new WHO Air Quality Guidelines. *J. Glob. Health* **2022**, *12*, 05043. [CrossRef]
49. Mezoue, C.A.; Ngangmo, Y.C.; Choudhary, A.; Monkam, D. Measurement of fine particle concentrations and estimation of air quality index (AQI) over northeast Douala, Cameroon. *Environ. Monit. Assess.* **2023**, *195*, 8. [CrossRef] [PubMed]
50. Svertoka, E.; Bălănescu, M.; Suciu, G.; Pasat, A.; Drosu, A. Decision Support Algorithm Based on the Concentrations of Air Pollutants Visualization. *Sensors* **2020**, *20*, 5931. [CrossRef] [PubMed]
51. Ouma, Y.O.; Keitsile, A.; Lottering, L.; Nkwae, B.; Odirile, P. Spatiotemporal empirical analysis of particulate matter $PM_{2.5}$ pollution and air quality index (AQI) trends in Africa using MERRA-2 reanalysis datasets (1980–2021). *Sci. Total Environ.* **2024**, *912*, 169027. [CrossRef] [PubMed]
52. Franceschi, F.; Cobo, M.; Figueredo, M. Discovering relationships and forecasting PM10 and PM2.5 concentrations in Bogotá, Colombia, using Artificial Neural Networks, Principal Component Analysis, and k-means clustering. *Atmos. Pollut. Res.* **2018**, *9*, 912–922. [CrossRef]
53. Gupta, P.; Christopher, S.A. Particulate matter air quality assessment using integrated surface, satellite, and meteorological products: Multiple regression approach. *J. Geophys. Res. Atmos.* **2009**, *114*, D14205. [CrossRef]
54. Romero, Y.; Chicchon, N.; Duarte, F.; Noel, J.; Ratti, C.; Nyhan, M. Quantifying and Spatial Disaggregation of Air Pollution Emissions from Ground Transportation in a Developing Country Context: Case Study for the Lima Metropolitan Area in Peru. *Sci. Total Environ.* **2020**, *698*, 134313. [CrossRef]
55. Bedregal, P.; Ubillus, M.; Cáceres-Rivero, C.; Olivera, P.; Garay, R.; Rojas, J.; Zafra, R.; Urdanivia, R. Determination of atmospheric aerosol components in an urban area to evaluate the air quality and identify the sources of contamination. *J. Radioanal. Nucl. Chem.* **2023**, *332*, 3507–3514. [CrossRef]
56. UNESCO. City of Cuzco, Peru, Inscribed in 1983 on the World Heritage List. UNESCO World Heritage Centre. 1983. Available online: https://whc.unesco.org/es/list/273 (accessed on 4 December 2024).
57. Morillas, H.; Gredilla, A.; Carrero, J.A.; Huallparimachi, G.; Gallego-Cartagena, E.; Maguregui, M.; Marcaida, I.; Astete, F.; Madariaga, J.M. Impact assessment of metals on soils from Machu Picchu archaeological site. *Chemosphere* **2020**, *242*, 125249. [CrossRef]
58. Morillas, H.; Maguregui, M.; Gallego-Cartagena, E.; Marcaida, I.; Carral, N.; Madariaga, J.M. The influence of marine environment on the conservation state of Built Heritage: An overview study. *Sci. Total Environ.* **2020**, *745*, 140899. [CrossRef] [PubMed]
59. Costantini, I.; Castro, K.; Madariaga, J.M.; Arana, G. Analytical Techniques Applied to the Study of Industrial Archaeology Heritage: The Case of Plaiko Zubixe Footbridge. *Molecules* **2022**, *27*, 3609. [CrossRef] [PubMed]
60. PRAL. Programa Regional de Aire Limpio. 2006. Available online: https://core.ac.uk/download/pdf/48031408.pdf (accessed on 4 December 2024).
61. Warthon, J.; Alvarez, M.; Olarte, A.; Quispe, Y.; Jalixto, V.; Valencia, N.; Mio-Diaz, M.; Zamalloa, A.; Warthon, B. Reduction of the concentration of particulate material at a sampling point in Cusco city at the beginning of the pandemic. *Sci. Rep.* **2024**, *14*, 849. [CrossRef]
62. Ceylan, Z.; Bulkan, S. Forecasting PM10 levels using ANN and MLR: A case study for Sakarya city. *Glob. Nest J.* **2018**, *20*, 281–290. [CrossRef]
63. Özdemir, U.; Taner, S. Impacts of Meteorological Factors on PM10: Artificial Neural Networks (ANN) and Multiple Linear Regression (MLR) Approaches. *Environ. Forensics* **2014**, *15*, 329–336. [CrossRef]
64. Ramli, N.; Hamid, H.A.; Yahaya, A.S.; Ul-Saufie, A.Z.; Noor, N.M.; Seman, N.A.; Kamarudzaman, A.N.; Deák, G. Performance of Bayesian Model Averaging (BMA) for Short-Term Prediction of PM10 Concentration in the Peninsular Malaysia. *Atmosphere* **2023**, *14*, 311. [CrossRef]
65. Kamarul Zaman, N.A.; Kanniah, K.D.; Kaskaoutis, D.G. Estimating Particulate Matter using satellite based aerosol optical depth and meteorological variables in Malaysia. *Atmos. Res.* **2017**, *193*, 142–162. [CrossRef]
66. Zateroglu, M.T. Forecasting particulate matter concentrations by combining statistical models. *J. King Saud Univ. Sci.* **2024**, *36*, 103090. [CrossRef]
67. Zaini, N.; Ahmed, A.N.; Ean, L.W.; Chow, M.F.; Malek, M.A. Forecasting of fine particulate matter based on LSTM and optimization algorithm. *J. Clean. Prod.* **2023**, *427*, 139233. [CrossRef]
68. Zhao, R.; Gu, X.; Xue, B.; Zhang, J.; Ren, W. Short period PM2.5 prediction based on multivariate linear regression model. *PLoS ONE* **2018**, *13*, e0201011. [CrossRef]
69. Srivastava, C.; Singh, S.; Singh, A.P. Estimation of air pollution in Delhi using machine learning techniques. *Int. Conf. Comput. Power Commun. Technol.* **2019**, 304–309. [CrossRef]
70. Domínguez-García, R.; Arellano-Vázquez, M. Evaluation of Machine Learning Models for Ozone Concentration Forecasting in the Metropolitan Valley of Mexico. *Appl. Sci.* **2024**, *14*, 1408. [CrossRef]

71. Ke, H.; Gong, S.; He, J.; Zhang, L.; Cui, B.; Wang, Y.; Mo, J.; Zhou, Y.; Zhang, H. Development and application of an automated air quality forecasting system based on machine learning. *Sci. Total Environ.* **2022**, *806*, 151204. [CrossRef]
72. Wang, J.; Wu, T.; Mao, J.; Chen, H. A forecasting framework on fusion of spatiotemporal features for multi-station PM2.5. *Expert Syst. Appl.* **2024**, *238*, 121951. [CrossRef]
73. Hoek, G.; Beelen, R.; de Hoogh, K.; Vienneau, D.; Gulliver, J.; Fischer, P.; Briggs, D. A review of land-use regression models to assess spatial variation of outdoor air pollution. *Atmos. Environ.* **2008**, *42*, 7561–7578. [CrossRef]
74. Tella, A.; Balogun, A.L.; Faye, I. Spatio-temporal modelling of the influence of climatic variables and seasonal variation on PM10 in Malaysia using multivariate regression (MVR) and GIS. *Geomat. Nat. Hazards Risk* **2021**, *12*, 443–468. [CrossRef]
75. Valle Díaz, F.R.; HuamánRomaní, Y.L. Análisis predictivo de los indicadores macroeconómicos del sector turístico post-Covid-19, Perú 2019–2023. *Rev. Venez. Gerenc.* **2022**, *27*, 580–596. [CrossRef]
76. Instituto Nacional de Estadística e Informática. Estadística Temática Turismo. INEI. 2024. Available online: https://www.inei.gob.pe/estadisticas/indice-tematico/turismo-11176/ (accessed on 4 December 2024).
77. Instituto Nacional de Estadística e Informática. Resultados Definitivos. INEI. 2018; pp. 24–25. Available online: https://www.inei.gob.pe/media/MenuRecursivo/publicaciones_digitales/Est/Lib1559/08TOMO_01.pdf (accessed on 4 December 2024).
78. U.S. Environmental Protection Agency. Guideline on Speciated Particulate Monitoring. US EPA. 1998. Available online: https://www3.epa.gov/ttnamti1/files/ambient/pm25/spec/drispec.pdf (accessed on 4 December 2024).
79. U.S. Environmental Protection Agency. Monitoring Regulations. US EPA. 2024. Available online: https://www.epa.gov/amtic/monitoring-regulations (accessed on 4 December 2024).
80. Blazkova, B.; Pastorkova, A.; Solansky, I.; Veleminsky, M., Jr.; Veleminsky, M.; Urbancova, K.; Vondraskova, V.; Hajslova, J.; Pulkrabova, J.; Sram, R.J. Effect of polycyclic aromatic hydrocarbons exposure on cognitive development in 5 years old children. *Brain Sci.* **2020**, *10*, 619. [CrossRef] [PubMed]
81. Trzyna, A.; Rybak, J.; Górka, M.; Olszowski, T.; Kamińska, J.A.; Węsierski, T.; Majder-Łopatka, M. Comparison of active and passive methods for atmospheric particulate matter collection: From case study to a useful biomonitoring tool. *Chemosphere* **2023**, *334*, 139004. [CrossRef]
82. Yang, L.; Shang, Y.; Hannigan, M.P.; Zhu, R.; Wang, Q.; Qin, C.; Xie, M. Collocated speciation of PM2.5 using tandem quartz filters in northern nanjing, China: Sampling artifacts and measurement uncertainty. *Atmos. Environ.* **2021**, *246*, 118066. [CrossRef]
83. U.S. Environmental Protection Agency. Compendium of Methods for the Determination of Inorganic Compounds in Ambient Air, Compendium Method IO-3.1: Selection, Preparation and Extraction of Filter Material. EPA/625/R-96/010a. 1999. Available online: https://www.epa.gov/sites/default/files/2015-07/documents/epa-io-3.1.pdf (accessed on 4 December 2024).
84. Lv, J.; Liu, S.; Li, Y. Spatial and seasonal variations of elemental and ion components in air particulate matters in three mega-cities in China. *Environ. Forensics* **2019**, *20*, 1–12. [CrossRef]
85. Jithin, J.; Srimuruganandam, B.; Nagendra, S.M.S. Characterization of PM10 and PM2.5 Emission Sources at Chennai, India. *Nat. Environ. Pollut. Technol.* **2019**, *2*, 555–562.
86. Afotey, B.; Sattler, M.; Parsaeifard, N.; Pearson, Y.E.; Chakraborty, M.; Hada, S. Impact of Corona Virus Stay-at-Home Policies on Traffic Emissions and Ambient Pollutant Concentrations in Ghana, West Africa. *Eng. Sci.* **2022**, *17*, 285–291. [CrossRef]
87. Chang, M.C.O.; Chow, J.C.; Watson, J.G.; Glowacki, C.; Sheya, S.A.; Prabhu, A. Characterization of Fine Particulate Emissions from Casting Processes. *Aerosol Sci. Technol.* **2005**, *39*, 947–959. [CrossRef]
88. Gu, Y.; Wylie, B.K.; Boyte, S.P.; Picotte, J.; Howard, D.M.; Smith, K.; Nelson, K.J. An Optimal Sample Data Usage Strategy to Minimize Overfitting and Underfitting Effects in Regression Tree Models Based on Remotely-Sensed Data. *Remote Sens.* **2016**, *8*, 943. [CrossRef]
89. Borrohou, S.; Fissoune, R.; Badir, H. Data cleaning survey and challenges—Improving outlier detection algorithm in machine learning. *J. Smart Cities Soc.* **2023**, *2*, 125–140. [CrossRef]
90. Alotaibi, O.; Pardede, E.; Tomy, S. Cleaning Big Data Streams: A Systematic Literature Review. *Technologies* **2023**, *11*, 101. [CrossRef]
91. Gudivada, V.N.; Apon, A.; Ding, J. Data Quality Considerations for Big Data and Machine Learning: Going Beyond Data Cleaning and Transformations. *Int. J. Adv. Softw.* **2017**, *10*, 1–20.
92. Ordoñez-Aquino, C.; Gonzales, G.F. Calidad del aire en Perú no se ajusta a los valores recomendados por la Organización Mundial de la Salud (OMS). *Rev. Med. Hered.* **2023**, *34*, 236–238. [CrossRef]
93. U.S. Environmental Protection Agency. Technical Assistance Document for the Reporting of Daily Air Quality—The Air Quality Index (AQI). EPA-454/B-24-002. 2024. Available online: https://document.airnow.gov/technical-assistance-document-for-the-reporting-of-daily-air-quailty.pdf (accessed on 4 December 2024).
94. Kebe, M.; Traore, A.; Manousakas, M.I.; Vasilatou, V.; Ndao, A.S.; Wague, A.; Eleftheriadis, K. Source Apportionment and Assessment of Air Quality Index of PM2.5–10 and PM2.5 in at Two Different Sites in Urban Background Area in Senegal. *Atmosphere* **2021**, *12*, 182. [CrossRef]

95. Karimian, H.; Li, Y.; Chen, Y.; Wang, Z. Evaluation of different machine learning approaches and aerosol optical depth in PM2.5 prediction. *Environ. Res.* **2023**, *216*, 114465. [CrossRef]
96. Wong, P.Y.; Lee, H.Y.; Zeng, Y.T.; Chern, Y.R.; Chen, N.T.; Lung, S.C.C.; Su, H.J.; Wu, C.D. Using a land use regression model with machine learning to estimate ground level PM2.5. *Environ. Pollut.* **2021**, *277*, 116846. [CrossRef] [PubMed]
97. Flatt, C.; Jacobs, R.L. Principle Assumptions of Regression Analysis: Testing, Techniques, and Statistical Reporting of Imperfect Data Sets. *Adv. Dev. Hum. Resour.* **2019**, *21*, 484–502. [CrossRef]
98. Miranda Hankgo, I.C.; Warthon Olarte, B.S.; Zamalloa Ponce de Leon, A.I.; Warthon Ascarza, J.L.; Olarte Perez, A.; Warthon Olarte, G.L.; Ramos Salcedo, V.F. Environmental impact by particulate material and meteorological parameters on the incidence of positive cases of COVID-19 during the first year of the pandemic in a high Andean city. *Earth Syst. Environ.* **2024**, *8*, 1267–1289. [CrossRef]
99. Kumar, P.; Hama, S.; Omidvarborna, H.; Sharma, A.; Sahani, J.; Abhijith, K.V.; Debele, S.E.; Zavala-Reyes, J.C.; Barwise, Y.; Tiwari, A. Temporary reduction in fine particulate matter due to 'anthropogenic emissions switch-off' during COVID-19 lockdown in Indian cities. *Sustain. Cities Soc.* **2020**, *62*, 102382. [CrossRef] [PubMed]
100. Sharma, A.K.; Balyan, P. Air pollution and COVID-19: Is the connect worth its weight? *Indian J. Public Health* **2020**, *64*, S132–S134. [CrossRef]
101. Wang, P.; Chen, K.; Zhu, S.; Wang, P.; Zhang, H. Severe air pollution events not avoided by reduced anthropogenic activities during COVID-19 outbreak. *Resour. Conserv. Recycl.* **2020**, *158*, 104814. [CrossRef] [PubMed]
102. Benchrif, A.; Wheida, A.; Tahri, M.; Shubbar, R.M.; Biswas, B. Air quality during three covid-19 lockdown phases: AQI, PM2.5 and NO2 assessment in cities with more than 1 million inhabitants. *Sustain. Cities Soc.* **2021**, *74*, 103170. [CrossRef] [PubMed]
103. Su, Y.; Li, J.; Liu, L.; Guo, X.; Huang, L.; Hu, M. Application of CNN-LSTM Algorithm for PM2.5 Concentration Forecasting in the Beijing-Tianjin-Hebei Metropolitan Area. *Atmosphere* **2023**, *14*, 1392. [CrossRef]
104. Li, X.; Ma, Y.; Wang, Y.; Liu, N.; Hong, Y. Temporal and spatial analyses of particulate matter (PM10 and PM2.5) and its relationship with meteorological parameters over an urban city in northeast China. *Atmos. Res.* **2017**, *198*, 185–193. [CrossRef]
105. Duarte, A.L.; Schneider, I.L.; Artaxo, P.; Oliveira, M.L.S. Spatiotemporal assessment of particulate matter (PM10 and PM2.5) and ozone in a Caribbean urban coastal city. *Geosci. Front.* **2022**, *13*, 101168. [CrossRef]
106. Carvalho, J.S.; Nascimento, R.K.S.; Cintra, J.V.F.R.F.; Rosa, N.L.C.; Grosseli, G.M.; Fadini, P.S.; Urban, R.C. Source apportionment and health impact assessment of atmospheric particulate matter in the city of São Carlos, Brazil. *Chemosphere* **2023**, *326*, 138450. [CrossRef]
107. Zeeshan, N.; Murtaza, G.; Ahmad, H.R.; Awan, A.N.; Shahbaz, M.; Freer-Smith, P. Particulate and gaseous air pollutants exceed WHO guideline values and have the potential to damage human health in Faisalabad, Metropolitan, Pakistan. *Environ. Monit. Assess.* **2024**, *196*, 659. [CrossRef] [PubMed]
108. Bao, R.; Zhang, A. Does lockdown reduce air pollution? Evidence from 44 cities in northern China. *Sci. Total Environ.* **2020**, *731*, 139052. [CrossRef]
109. Abulude, F.O.; Akinnusotu, A.; Bello, L.; Feyisetan, A.O. Assessment of AQI, PM10, PM2.5, NO2, O3: The Case of OWO, Nigeria. *ASEAN J. Sci. Eng.* **2024**, *4*, 15–24. [CrossRef]
110. Zaib, S.; Lu, J.; Bilal, M. Spatio-Temporal Characteristics of Air Quality Index (AQI) over Northwest China. *Atmosphere* **2022**, *13*, 375. [CrossRef]
111. Aishan, T.; Sun, Y.; Halik, Ü.; Betz, F.; Yusup, A.; Rezhake, R. Spatiotemporal changes in fine particulate matter and ozone in the oasis city of Korla, northeastern Tarim Basin of China. *Sci. Rep.* **2024**, *14*, 1–12. [CrossRef] [PubMed]
112. Behnood, A.; Daneshvar, D. A machine learning study of the dynamic modulus of asphalt concretes: An application of M5P model tree algorithm. *Constr. Build. Mater.* **2020**, *262*, 120544. [CrossRef]
113. Behnood, A.; Behnood, V.; Gharehveran, M.M.; Alyamac, K.E. Prediction of the compressive strength of normal and high-performance concretes using M5P model tree algorithm. *Constr. Build. Mater.* **2017**, *142*, 199–207. [CrossRef]
114. Behnood, A.; Olek, J.; Glinicki, M.A. Predicting modulus elasticity of recycled aggregate concrete using M5′ model tree algorithm. *Constr. Build. Mater.* **2015**, *94*, 137–147. [CrossRef]
115. Kumar, K.; Pande, B.P. Air pollution prediction with machine learning: A case study of Indian cities. *Int. J. Environ. Sci. Technol.* **2023**, *20*, 5333–5348. [CrossRef]
116. Polcyn, J.; Voumik, L.C.; Ridwan, M.; Ray, S.; Vovk, V. Evaluating the Influences of Health Expenditure, Energy Consumption, and Environmental Pollution on Life Expectancy in Asia. *Int. J. Environ. Res. Public Health* **2023**, *20*, 4000. [CrossRef] [PubMed]
117. Alsaber, A.R.; Pan, J.; Al-Hurban, A. Handling Complex Missing Data Using Random Forest Approach for an Air Quality Monitoring Dataset: A Case Study of Kuwait Environmental Data (2012 to 2018). *Int. J. Environ. Res. Public Health* **2021**, *18*, 1333. [CrossRef]
118. Pyae, T.S.; Kallawicha, K. First temporal distribution model of ambient air pollutants (PM2.5, PM10, and O3) in Yangon City, Myanmar during 2019–2021. *Environ. Pollut.* **2024**, *347*, 123718. [CrossRef] [PubMed]

119. Galán-Madruga, D.; Broom, I.P.; Satyanaga, A.; Jahanbakhshi, A.; Bagheri, M.; Fathian, A.; Sarvestan, R.; Cárdenas-Escudero, J.; Cáceres, J.O.; Kumar, P.; et al. A methodological framework for estimating ambient PM2.5 particulate matter concentrations in the UK. *J. Environ. Sci.* **2025**, *150*, 676–691. [CrossRef]
120. Raju, L.; Gandhimathi, R.; Mathew, A.; Ramesh, S.T. Spatio-temporal modelling of particulate matter concentrations using satellite derived aerosol optical depth over coastal region of Chennai in India. *Ecol. Inform.* **2022**, *69*, 101681. [CrossRef]

Disclaimer/Publisher's Note: The statements, opinions and data contained in all publications are solely those of the individual author(s) and contributor(s) and not of MDPI and/or the editor(s). MDPI and/or the editor(s) disclaim responsibility for any injury to people or property resulting from any ideas, methods, instructions or products referred to in the content.